Politecnico di Torino

Politecnico di Torino

Master's degree programme in Aerospace Engineering
A.a. 2023/2024
Graduation session December 2024

Experimental study on the effect of density ratio on the rotor-stator disc cavity purge flow

Supervisors:
Salvadori Simone
Misul Daniela Anna
Fridh Jens

Candidate:
Lapioli Alberto Maria

Author

Alberto Maria Lapioli
amlap@kth.se, s305529@studenti.polito.it
Master Thesis student at KTH Royal Institute of Technology, student at Politecnico di Torino

Place for Project

KTH - Division of Heat and Power Technology
Brinellvägen 68, 114 28 Stockholm, Sweden

KTH supervisor

Jens Fridh
jensa@kth.se
Researcher at the Division of Heat and Power Technology
KTH Royal Institute of Technology

PoliTO supervisors

Simone Salvadori
simone.salvadori@polito.it
Professor at the Department of Energy
Politecnico di Torino

Daniela Anna Misul
daniela.misul@polito.it
Professor at the Department of Energy
Politecnico di Torino

When things are not working out, remind yourself that the opportunity to study is a privilege not everyone gets. It will help you face and solve challenges.

Abstract

The ingestion of hot mainstream through the rim seal of a high-pressure turbine stage can be controlled by the so-called cavity purge flow. It is a cooling flow of pressurized air introduced into the wheel space between the stator and rotor disks, which then interacts with the main annulus flow via the rim seal. In gas turbines there is a temperature difference between these two flows and thus a density ratio that affects the effectiveness of the rim seal. Also, the purge flow reduces turbine efficiency. The purpose of this thesis is to study the density ratio influence of the cavity purge flow, mainly in terms of sealing effectiveness and the effect on other relevant cavity flow parameters. The study was carried out through the KTH Test Turbine, that is a joint venture between Siemens Energy and KTH. The investigated turbine stage is a low degree of reaction high pressure axial turbine and the useful flow details are taken through pneumatic and temperature probes. The stage was tested under varying purge flow densities created by flowing air (DR=1) or argon (DR=1.38) into the cavity, and for three different mass flow ratios (MFR), both at the design point and off-design. To evaluate the sealing effectiveness, trace gas measurements of CO_2 are performed in the cavity. For the same value of purge mass flow (i.e. MFR), the use of a purge gas characterized by a higher density ratio results in lower effectiveness values. In off-design conditions, the sealing level increases. As for the efficiency, total-to-total and total-to-static efficiency have been plotted; the trend is decreasing with the increase of the MFR, as expected, regardless of the gas used as purge. For the same MFR, the use of an heavier purge gas appears to result in lower efficiency values, apart from the higher MFR, both at the design point and off-design. The experimental data obtained could be used to calibrate correlations and models developed in the past few years. In this regard, the Orifice Model was used to interpolate the experimental data in order to find the optimal value for the discharge coefficient, which characterizes the rim seal, confirming results in literature. As the last, the swirl ratio was calculated to check whether any compressibility effect occurs within the cavity; observing the values of the swirl Mach number, it can be concluded that no major compressibility effects occur. The results of this work can be useful to predict the appropriate amount of purge to achieve a good trade-off between efficiency and safe operating temperatures. Also, to extrapolate test rig results to engine operating conditions.

Keywords

turbomachinery; axial turbine; cooling; cavity purge flow; density ratio; wheel space; rim seal; gas sampling; sealing effectiveness; efficiency; Orifice Model; swirl ratio

Sammanfattnig

Inträngningen av varm huvudström genom fälgtätningen i ett högtrycksturbinsteg kan kontrolleras med hjälp av det så kallade cavity purge-flödet. Det är ett kylflöde av tryckluft som förs in i hjulutrymmet mellan stator- och rotorskivorna och som sedan samverkar med huvudringflödet via fälgtätningen. I gasturbiner finns det en temperaturskillnad mellan dessa två flöden och därmed ett densitetsförhållande som påverkar fälgtätningens effektivitet. Dessutom minskar reningsflödet turbinens verkningsgrad. Syftet med denna avhandling är att studera densitetskvotens inverkan på kavitetsflödet, främst när det gäller tätningseffektivitet och effekten på andra relevanta kavitetsflödesparametrar. Studien genomfördes med hjälp av KTH Test Turbine, som är ett joint venture mellan Siemens Energy och KTH. Det undersökta turbinsteget är en högtrycksaxialturbin med låg reaktionsgrad och de användbara flödesdetaljerna tas genom pneumatiska och temperaturprober. Steget testades under varierande spolningsflödestätheter som skapades genom att luft eller argon flödade in i kaviteten, och för tre olika massflödeskvoter (MFR), både vid designpunkten och utanför designen. För att utvärdera tätningseffektiviteten utförs spårgasmätningar av CO_2 i kaviteten. För samma massflödesvärde (dvs. MFR) resulterar användning av en spolgas med högre densitet i lägre effektivitetsvärden. Under förhållanden som inte överensstämmer med konstruktionen ökar tätningsnivån. När det gäller verkningsgraden har total-till-total och total-till-statisk verkningsgrad plottats; trenden är som väntat minskande med ökande MFR, oavsett vilken gas som används som spolgas. För samma MFR verkar användningen av en tyngre spolgas resultera i lägre verkningsgrader, bortsett från den högre MFR, både vid designpunkten och utanför designpunkten. De experimentella data som erhållits kan användas för att kalibrera korrelationer och modeller som utvecklats under de senaste åren. I detta avseende användes Orifice Modellen för att interpolera de experimentella data för att hitta det optimala värdet för urladdningskoefficienten, som kännetecknar fälgtätningen, vilket bekräftar resultat i litteraturen. Sist beräknades virvelförhållandet för att kontrollera om någon kompressionseffekt uppstår i kaviteten; genom att observera värdena för virvelns Mach-tal kan man dra slutsatsen att inga större kompressionseffekter uppstår. Resultaten av detta arbete kan vara användbara för att förutsäga lämplig mängd rening för att uppnå en bra avvägning mellan effektivitet och säkra driftstemperaturer. De kan också användas för att extrapolera resultaten från testriggen till motorns driftsförhållanden.

Nyckelord

strömningsmaskiner; axialturbin; kylning; kavitetsrensningsflöde; densitetskvot; hjulutrymme; kanttätning; gasprovtagning; tätningens effektivitet; verkningsgrad; Orifice Modellen; virvelförhållande

Acknowledgements

Looking back over the years, I perfectly remember when I chose to start my university period in Turin. It was a couple of days before classes started and I was undecided whether to go to Turin or to a city closer to my hometown. Even, I would not have imagined that I could go even further away until I got to Sweden. After these years, I can say that it was worth it. Be away from my hometown, my family and my childhood friends has helped me grow and be more mature. However, it sounds like I am describing them as sacrifices but they are not at all. On the contrary, it was a privilege for which I have to thank my parents who allowed me to study away from home and never let me lack anything. Initially I did not think about this, but now that I am more mature I realize that it is an opportunity that not everyone gets, and for that I especially thank my father. Also, thanks to my older brother, you have been a point of reference, as shown by the fact that, like you, I studied both in Turin and Stockholm; you have always been available to give me any kind of advice, university or not.

If I had the opportunity to study in Stockholm, part of the credit is also due to those who allowed me to do a thesis abroad under their guidance. First, I would like to thank my supervisor Jens who replied to my e-mail when I asked for a master's thesis. You were always available in welcoming me to your office at all times to discuss about my doubts; above all, thank you for always telling me that I am the "driver" of my thesis, it helped me to take responsibility. Thanks to Navid, Sebastian and the others from Siemens; you gave me the opportunity to collaborate with industry by attending project meetings, and now I realize it was a great experience to have during my time at university. Thanks to Tim, who started his thesis two months before me so was helpful in giving me tips whenever I needed it; we had fun times together in assembling the Test Turbine and joked during our days in the lab. Thanks to the lab technicians Leif and Emil, without whom testing would not have been possible. Thanks to Carlos, Jules, Nenad and Salvatore who supported me when things were not working out, to Taras who helped me calibrate the gas analyzer, and especially to Steffen for the productive chats together and always trying to help me figuring out some of the problems even if they were not within his competence. Thanks to all the previous researchers who worked on the test rig, your work was very helpful. Thanks to my Italian supervisors, Daniela and Simone; I know it has been difficult to collaborate remotely, but I have done my best to keep you updated. Also, from a mistake I made during a meeting with you, I learnt that I must prepare a presentation for every

future meeting.

When I arrived in Turin, I already had friends, so it was easy to settle in and meet new friends. We shared many good times together, from nights out to futsal games to jokes about our ”enemy” home provinces. But, before arriving in Stockholm, I was scared about starting a new life in a new country, with a new language and, above all, alone. Nevertheless, with some time, I was able to make new friends without whom I could never have enjoyed the best time of my life so far so much. We shared so many things together that made these six months feel like a vacation. It would be too long to list all of your names, but you know that I am talking about the group of friends on Erasmus and those with whom I have shared the last two months; most importantly, you know that there are no better words than those I have said to describe how important you have been. Also, thanks to all my friends from my teenage years in Italy; even though we were far away during my university years, I always thought of you and you can notice it by how happy I was every time I went back to see you again and share once again those moments that I could never share with anyone else and, most of all, by how sad I was every time I had to leave.

Nomenclature

Symbol	Description	Unit	Definition
a	wheel space axial clearance	m	
b	disc outer radius	m	
C_d	discharge coefficient	-	
CF	conversion factor	-	Eq. 53
C_f	flow coefficient	-	Eq. 33
C_w	non-dimensional flow rate	-	Eq. 26
c	absolute flow velocity	m/s	Eq. 3
c_p	heat capacity at constant pressure	$J/(kg \cdot K)$	
d	disc inner radius	m	
G	gap ratio	-	Eq. 23
G_s	seal clearance ratio	-	Eq. 27
$\dot{m}$	mass flow rate	kg/s	Eq. 2
h	enthalpy	J/kg	
p	pressure	Pa	
Q	specific heat	J/kg	
Re_{c_x}	axial Reynolds number	-	Eq. 32
Re_θ	rotational Reynolds number	-	Eq. 22-28
r	radius	m	
s	seal clearance	m	
U	mean purge flow velocity	m/s	Eq. 30
u	rotor blade speed	m/s	
W	specific work	J/kg	Eq. 8-9-10
w	relative flow velocity	m/s	
x_{corr}	corrected radial position	-	Eq. 48
α	absolute flow angle	deg	
β	relative flow angle	deg	
β	swirl ratio	-	Eq. 24
β^*	swirl ratio when $C_w = 0$	-	
Γ_c	ratio of discharge coefficients	-	Eq. 42
γ	seedgas concentration	$\%_{vol}$	
ΔC_p	non-dimensional pressure difference	-	Eq. 25
Δp	peak-to-trough pressure difference	Pa	
ε	sealing effectiveness	-	Eq. 34
η	efficiency	-	Eq. 17 - 18
κ	ratio of specific heats	-	
Λ	degree of reaction	-	Eq. 13 - 14
λ_t	turbulent flow parameter	-	Eq. 49
μ	dynamic viscosity	$Pa \cdot s$	
π	pressure ratio	-	
ν	isentropic velocity ratio	-	Eq. 16
ρ	density	kg/m^3	
τ	torque	$N \cdot m$	Eq. 6

Symbol	Description	Unit	Definition
Φ	non-dimensional sealing parameter	-	Eq. 29-31
ϕ	flow coefficient	-	Eq. 11
ψ	stage loading	-	Eq. 12
Ω	rotor angular velocity	rad/s	
ω	core angular velocity	rad/s	

Subscripts	Description
o	purge flow
0	total condition
1	stator inlet
2	stator outlet and rotor inlet
3	rotor outlet
CI	Combined Induced ingestion
EI	Externally Induced ingestion
e	egress
i	ingress
is	isoentropic transformation
m	meridian component
min	minimum
RI	Rotationally Induced ingestion
r	rotor
s	stator
x	axial direction
θ	tangential direction

Acronyms	Description	Unit	Definition
DR	density ratio	-	Eq. 43
MFR	mass flow ratio	-	Eq. 52
MFC	mass flow controller		
OM	Orifice Model		
CFD	Computational Fluid Dynamics		

List of Figures

List of Tables

Contents

1 Introduction

Gas turbines are very widespread nowadays, being applied to aero-propulsion, ship power and industrial power generation. They are devices designed to convert the thermal energy of a fuel into some form of useful power, such as electricity, mechanical power for ship propulsion or highspeed thrust in an aircraft jet engine [1], [2]. However, gas turbines are responsible for global emissions of CO_2 in the atmosphere. Over the years, improvements have focused on increasing turbine efficiency so that CO_2 emissions are reduced. In this regard, flow mixing and cooling have been identified as areas that would benefit from further research.

Regardless of the application, gas turbines are made of a gas generator and a power-conversion section. The gas generator consists of three principal components, usually mounted on a single shaft: compressor, combustion chamber and turbine. First, the flow passes through the compressor so that the pressure is increased. Next, the compressed flow goes into the combustion chamber, where is mixed with the added fuel and combustion takes place, thus raising the temperature. Then, the hot gases expand in the turbine to produce power. This power is used both to drive the compressor and to produce electricity (power generation plants) or thrust (aircraft). The secondary air system provides cooling air to critical parts, like turbine blades and vanes, combustion chamber, disks and bearing chambers. However, cooling has its own because coolant air is bled from the compressor, so it requires energy to be compressed but does not help to produce the cycle output. Also, the injection of cooling air within the main flow generates losses due to mixing.

Since the hot gases at the turbine inlet can reach very high temperatures that can stress turbine material, new materials and cooling techniques have been developed. Indeed, high temperatures mean good performance, but it is also important to protect the turbine, otherwise power generation cannot occur. There are several ways to cool down a turbine, such as film cooling, internal cooling, cavity cooling. The latter refers to the cooling of the space between stator and rotor disks (wheel space) through the so called cavity purge flow.

The cavity purge flow consists of a cavity of one rotating and one stationary wall. This system is then connected to a turbine annulus via a rim seal, as exemplified in Figure 1.1. An unpredicted ingestion of hot gas may harm temperature sensitive components in the turbine interior. To avoid hot gas ingestion, air is bled from the compressor and supplied

in the wheel space in order to pressurize it, and then leaves through the rim seal. However, this cavity purge flow has a negative impact on turbine efficiency. It is therefore important that it is minimized and avoided if not necessary. In gas turbines, a temperature difference exists between the cavity flow and the main annulus flow, leading to a density ratio that affects the sealing effectiveness of the rim seal. The design of the rim seal is also important in limiting the flow exchange between the two flows.

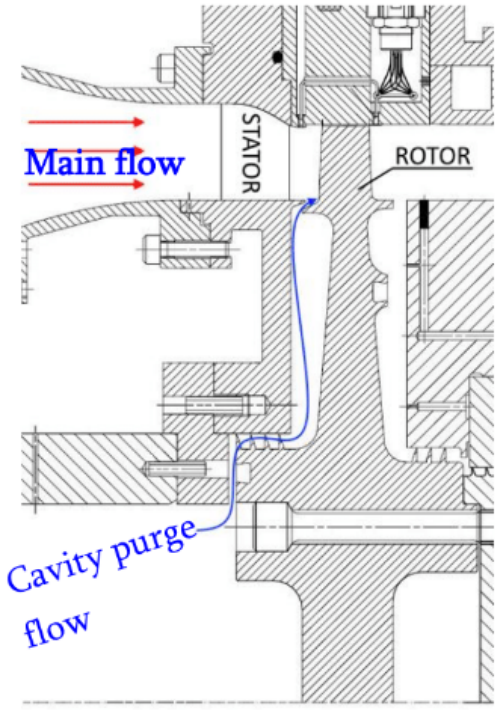

Figure 1.1: Cross-section of turbine stage, highlighting the cavity purge flow exiting from the wheel space, past the rim seal and into the main annulus

1.1 Background

A turbine is a rotating device that converts the energy in a stream of fluid into mechanical energy by changing its angular momentum. Conversion is done by passing the fluid through a fixed and a moving part, which together are called a stage. It is possible to have more than one stage. The fixed part is called the stator, the moving part is called the rotor. The goal of the stator is to redirect the fluid and to decrease its pressure and enthalpy to generate an increase in kinetic energy that is converted into work by the rotor, which turns the fluid and possibly continue its acceleration. Moving fluid acts on the rotor blades so that they move in the direction of rotation, generating the torque on the shaft. The latter reacts with a force of equal magnitude in the opposite direction: this force allows

to change the direction of flow and so its angular momentum [3].
The main annulus flow is radially bounded by the hub and the casing, respectively lower and upper limit. The wheel space is a cavity between stator and rotor disk, radially below the hub, which can take different geometries. Since there is a gap between the stator and rotor to allow rotor movement, it is important to prevent hot gas ingestion and so limit the fluid exchange between the cavity and the main annulus. To do so, a rim seal is commonly introduced in the hub region, either on stationary or rotating side, protruding toward the opposite side. To limit this fluid exchange, air can also be purged from the compressor and passed through the wheel space, then exiting via the rim seal. This allows the local temperature to be within safe limits, but it is detrimental to the efficiency of the turbine as the cold flow mixes with the hot main flow [3].

1.2 Problem

Since the purge flow is slower than the main annulus flow, mixing occurs between them and, consequently, entropy generation [4]. As the goal of a turbine is to produce the maximum possible amount of work through the rotor by converting kinetic energy, this shear mixing problem is dominant downstream of the stator as it accelerates the flow. In addition, the purge flow thickens the boundary layer on the rotor side, thereby strengthening the secondary vortex as the flow is turned through the rotor [3]. The main problem is that the interaction between main flow and purge flow has a negative impact on turbine efficiency, so it is necessary to find a trade-off between cooling and mixing effects, in order to minimize and avoid purge flow if unnecessary.

1.3 Purpose

The aim of the thesis is to study the density ratio influence of the cavity purge flow, mainly in terms of sealing effectiveness and the effect on other relevant cavity flow parameters. It is also important to predict the impact of the purge flow on turbine stage efficiency and to what extent the density ratio affects it. The study is mainly experimental and the measurements are performed using a turbine testing facility (hereafter referred to as the Test Turbine), whose stage under analysis is a low degree of reaction high pressure axial turbine. The experimental data obtained can be used to calibrate a model developed in recent literature.

1.4 Methodology

The thesis work requires to perform a series of experiments on the Test Turbine to collect data for analysis. Flow details are measured through pneumatic probes and thermocouples. To evaluate the sealing effectiveness, sampling measurements of a foreign gas such as CO_2 are performed in the cavity under varying purge flow density created by a mixture of air and argon. The data were processed primarily with MATLAB and, when possible, also with Excel to have a double check. Once the sealing effectiveness is calculated, the Orifice Model can be used to interpolate the experimental data in order to find the optimal value for the discharge coefficient, which characterizes the rim seal. Two version of this model were used, one without DR and one taking into account the effect of DR. To evaluate the efficiency, an online Excel program developed by Siemens was used from which the values of the required enthalpies were taken. It is important to note that the mass flow controllers installed in the laboratory are calibrated for air, so to perform tests with argon as purge flow, a conversion factor between air and argon must be calculated.

1.5 Stakeholders

The work is carried out using the Test Turbine, which is part of an applied commissioned research project between KTH and Siemens Energy AB. The Test Turbine is located in the laboratory of the Unit of Heat and Power Technology at KTH.

1.6 Delimitations

During the work, different operating points and mass flow ratios have been studied. However, different turbine designs could not be studied because only an axial flow, low degree of reaction, high pressure turbine stage is available in the laboratory. Besides, only one stage and thus only one cavity was analyzed, although other cavities are subject to the risk of hot gas ingestion. However, the first cavity is critical because it is the first to be encountered by the hot flow and, after the first rotor, the temperature decreases. In addition, the flow velocity is higher at the stator-rotor interface than downstream of the rotor, so this area is sensitive to the injected purge flow [3].

1.7 Outline

Chapter 2 covers the theory of turbomachinery, dealing with both turbine main annulus flow and cavity purge flow, with a focus on the interaction between purge flow and secondary flows. Chapter 3 explains the research methodology and gives a practical description of how the methods were applied. Chapter 4 presents and analyzes the results, while Chapter 5 summarizes the key findings obtained throughout the project and outlines future work.

2 Theoretical Background

As said before in the section 1.3, this work foucuses on an axial turbine. Axial turbines are the most common turbine configuration for electric power generation and propulsion systems due to their versatility in terms of power capacity and range of operating conditions [5].

2.1 Generalities about turbine

2.1.1 Velocity triangles

Velocity triangles are used for the study of turbomachines within the framework of one-dimensional theory. Letter $\vec{c}$ denotes the velocity of the fluid with respect to a fixed reference system (i.e. inertial system), called absolute flow velocity. Letter $\vec{w}$ denotes the velocity of the fluid with respect to a non inertial reference system, called relative flow velocity. Letter $\vec{u}$ denotes how the midpoint of the rotor blade moves relative to the inertial reference system, so it is not related to the fluid and is called rotor blade speed. For each interface section between stator vane and rotor blade, velocity triangles are drawn in a plane identified by two directions that are always perpendicular to each other: meridian direction and tangential direction. The meridian section is obtained by sectioning the machine with a plane passing through the axis of the machine. In the latter section, it is possible to represent the so called meridian component of velocity c_m, defined as:

$$c_m = \vec{c} \cdot \vec{n} = c_r \vec{\lambda} + c_a \vec{\mu} \tag{1}$$

where $\vec{n}$ is the normal versor exiting the surface A, c_r and c_a are respectively the radial and axial components. Also, c_m is what gives the mass flow rate:

$$\dot{m} = \int_A \rho c_m \, dA \tag{2}$$

The absolute flow velocity can be written as:

$$\vec{c} = c_r \vec{\lambda} + c_a \vec{\mu} + c_u \vec{\nu} \tag{3}$$

in which c_u is the tangential component and, by definition, the three components are perpendicular to each other. Thus, the meridian component of velocity is perpendicular to the tangential one.
Regarding turbine stages, it is possible to distinguish between axial stage and radial stage:

- in axial stage, the meridian direction of the velocity coincides with the axial direction throughout the stage;
- in radial stage, the meridian direction of the velocity coincides with the radial direction throughout the stage.

The stage is mixed if the meridian direction has both components, axial and radial, and eventually these change along the stage. An example of a mixed stage is the centrifugal stage, in which the inlet direction is axial and the outlet direction is radial.
Another distinction is between action stage and reaction stage:

- in action stage there is no expansion through the rotor, thus $p_3 = p_2$;
- in reaction stage, there is expansion through the rotor, thus $p_3 < p_2$.

One-dimensional motion is a good approximation of reality for studying a turbine stage if the following conditions hold:

- blade height much less than the average diameter, so that $u_{root} \simeq u_{tip} \simeq u$;
- large number of blades, so that the circumferential length of the fluid passage channel is approximately equal when evaluated at the root and tip of the blade.

These conditions are very well verified in the high-pressure turbine stages, as shown in the Figure 2.1.

Figure 2.1: Example of a scaled high pressure turbine rotor

To draw the velocity triangles, two directions are drawn perpendicular to each other: the tangential direction (by convention drawn horizontally) and the meridian direction (by convention drawn vertically). On the plane identified by the latter directions lies the velocity vector of the fluid particle.

Figure 2.2 shows a radial view of a turbine stage, with vertical shaft direction and flow from top to bottom. In addition, velocity triangles are represented at the ingress and exit of both stator vane and rotor blade, at a certain representable radial level [3].

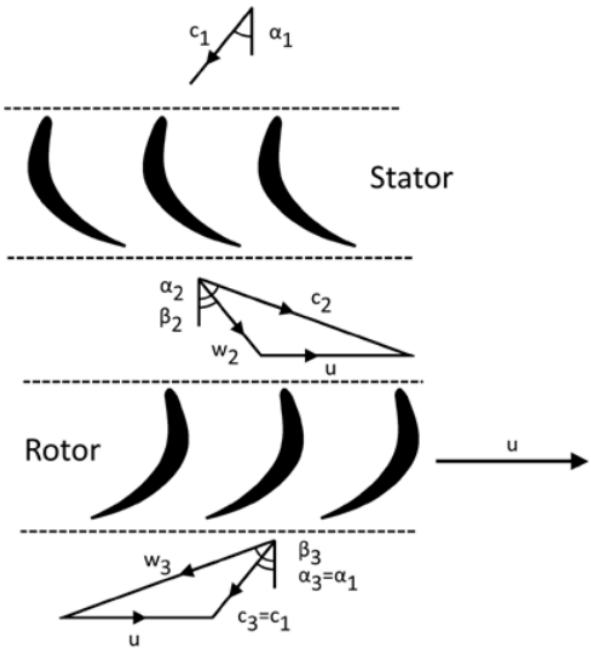

Figure 2.2: Schematic radial view of turbine stage. Adapted from [6]

As can be seen from Figure 2.2, the vector relationship between the velocities is as follows

$$\vec{c} = \vec{w} + \vec{u} \tag{4}$$

It is also possible to see the stator's goal to decrease pressure and enthalpy in order to increase kinetic energy, as $|\vec{c_2}| > |\vec{c_1}|$. Then, the relative flow (i.e. $\vec{w}$) enters the rotor aligned with the blade profile, where the gain of kinetic energy is transformed into work. Usually, the design choice is repeated stages so that the absolute velocity vector exiting the rotor is the same as that entering the stage, so $|\vec{c_3}| = |\vec{c_1}|$ and the exiting flow is aligned with the stator of the next stage.

Moving fluid acts on the rotor blades so that they move in the direction of rotation, generating the torque on the shaft, that reacts with a force of equal magnitude in the opposite direction [3]. This exchange of forces is taken into account by Newton's second law of motion, whereby the rate of change of momentum of a mass is equal to the sum of forces acting on it:

$$\sum \vec{F} = \frac{d}{dt}(m\vec{c}) \tag{5}$$

The torque is computed by applying Eq. 5 to the rotational direction, assuming steady massflow:

$$\tau = \dot{m}(r_3 \cdot c_{3\theta} - r_2 \cdot c_{2\theta}) \tag{6}$$

By multiplying Eq. 6 for the rotor angular velocity and considering that $u = \Omega r$, gives the following equation:

$$\tau\Omega = \dot{m}(u_3 \cdot c_{3\theta} - u_2 \cdot c_{2\theta}) \tag{7}$$

The first member of the Eq. 7 represents the shaft power, which is equal to the specific work times the mass flow rate. Thus, the specific work results to be:

$$W = u_3 \cdot c_{3\theta} - u_2 \cdot c_{2\theta} \tag{8}$$

With this formulation, the specific work is negative, so the convention is to change the sign to reflect the working principle of a turbine, which is to extract work from the fluid. Also, the rotor blade speed is usually constant, so it is possible to write $u = u_1 = u_2 = u_3$ and the Eq. 8 becomes:

$$W = u\left(c_{2\theta} - c_{3\theta}\right) \tag{9}$$

The specific work can also be expressed as the change of total enthalpy through the rotor. From the first principle of thermodynamics, assuming adiabatic flow, the total enthalpy change of the stage is derived exclusively to work. In addition, there is no change in total enthalpy in the stator since it extracts no work from the flow, so $h_{01} = h_{02}$. From this follows the Euler's turbine equation [3]:

$$W = h_{01} - h_{03} \tag{10}$$

2.1.2 Design parameters

In the field of turbomachinery, three non-dimensional design parameters are usually used: flow coefficient, stage loading and degree of reaction.
The flow coefficient ϕ is defined as the ratio between the absolute axial velocity and the rotor blade speed:

$$\phi = \frac{c_x}{u} = \frac{c_x}{\Omega \cdot r} \tag{11}$$

As can be seen from the Eq. 11, the flow coefficient should be defined at a convenient radial location and can vary with axial location. A high flow coefficient means flow velocities towards the axial direction, a low coefficient means flow velocities towards the tangential direction.
The stage loading ψ is defined as the ratio of twice the change in tangential velocity across the rotor to the speed of the rotor blades:

$$\psi = \frac{2(c_{2\theta} - c_{3\theta})}{u} = \frac{2(h_{01} - h_{03})}{u^2} \tag{12}$$

As can be seen from the Eq. 12, the stage loading can be expressed through the Euler's turbine equation (see Eq. 9 and Eq. 10), considering the same radial position.
The degree of reaction Λ is defined as the ratio of the static enthalpy drop across the rotor to the static enthalpy drop across the whole stage:

$$\Lambda = \frac{h_2 - h_3}{h_1 - h_3} \tag{13}$$

In an action turbine, $\Lambda = 0$ since $p_3 = p_2$ and therefore there is no enthalpy drop across the rotor. This could also be seen writing the Eq. 13 in terms of pressure drops. Indeed, assuming calorically perfect gas (i.e. constant heat capacity c_p, not dependent

on temperature), the enthalpy drop is directly proportional to the temperature drop, making the two effectively the same. Besides, assuming an adiabatic and isoentropic transformation, temperature drop can be replaced by pressure drop, leading to the Eq. 14:

$$\Lambda = \frac{T_2 - T_3}{T_1 - T_3} = \frac{p_2 - p_3}{p_1 - p_3} \tag{14}$$

The extreme value taken by the degree of reaction is $\Lambda = 0$, which means $h_2 = h_3$, so there is no expansion in the rotor but all of it happens in the stator. In other words, when $\Lambda = 0$, the rotor does not accelerate the flow but only redirects it. Therefore the relative velocities w_1 and w_2 have the same magnitude and, in the velocity triangles, this is shown through the equal but opposite sign of relative angles β_1 and β_2. By increasing the degree of reaction from the zero value, the rotor begins to accelerate the flow until the case where $\Lambda = 1$, in which $h_1 = h_2$ thus the acceleration all occurs in the rotor. An interesting case is when $\Lambda = 0,5$ since it means that the velocity triangles upstream and downstream of the rotor are symmetrical, so $\alpha_2 = \beta_1$ and $\alpha_1 = \beta_2$.

The degree of reaction and the flow coefficient are related by the following relationship:

$$\Lambda = \frac{\phi}{2}(\tan\beta_3 - \tan\beta_2) \tag{15}$$

Another useful non-dimensional coefficient is the isoentropic velocity ratio, denoted as ν, which is used to non-dimensionalize the rotational speed. Similar to the stage loading ψ, it relies on the same parameters, but instead of the real enthalpy change, it uses the isentropic total enthalpy change of the stage, along with the static outlet condition.

$$\nu_{tot-stat} = \frac{u}{\sqrt{2(h_{01} - h_3)}} \cong \frac{1}{\sqrt{\psi}} \tag{16}$$

The denominator of Eq. 16 quantifies the velocity gained via isoentropic acceleration from the inlet to the outlet condition [3].

2.1.3 Efficiency of a turbine stage

The efficiency is defined as the ratio between the real enthalpy change of the stage and the ideal isoentropic enthalpy change of the stage. There are two definitions that differ in the isoentropic part, and they depend on whether the kinetic energy at the output of the stage is fully utilized or fully dissipated before reaching the next stage.

If the kinetic energy at the output of the stage is fully utilized in the next stage, the total-to-total efficiency is defined as:

$$\eta_{tot-tot} = \frac{W}{W_{is_{tot-tot}}} = \frac{h_{01} - h_{03}}{(h_{01} - h_{03})_{is}} \tag{17}$$

In this case, the kinetic energy $\frac{c_3^2}{2}$ is not a loss and this occurs in an intermediate stage of a multi-stage machine with the next stage very close to the previous one.
If the kinetic energy at the output of the stage is fully dissipated, the total-to-static efficiency is defined as:

$$\eta_{tot-stat} = \frac{W}{W_{is_{tot-stat}}} = \frac{h_{01} - h_{03}}{(h_{01} - h_{3})_{is}} \tag{18}$$

In this case, the kinetic energy $\frac{c_3^2}{2}$ is a loss and this occurs in an intermediate stage of a multi-stage machine with the next stage far away.
The selection of which efficiency definition to use depends not only on how the kinetic energy at the stage's output is utilized, but also on the available output measurements. If the total outlet conditions cannot be accurately measured or are unreliable, the total-to-static efficiency is an alternative. For each definition, the isoentropic enthalpy drop is calculated assuming calorifically perfect gas (i.e. constant heat capacity c_p, not dependent on temperature), which is a good hypothesis for low temperatures [3]:

$$(h_{01} - h_{03})_{is} = c_p \cdot T_{01} \left[1 - \left(\frac{p_{03}}{p_{01}} \right)^{\frac{\kappa-1}{\kappa}} \right] \tag{19}$$

$$(h_{01} - h_{3})_{is} = c_p \cdot T_{01} \left[1 - \left(\frac{p_{3}}{p_{01}} \right)^{\frac{\kappa-1}{\kappa}} \right] \tag{20}$$

2.1.4 Ideal cycle

The ideal gas turbine considers a perfect gas as fluid and no losses. The reference cycle is the ideal Joule cycle, made of stationary and reversible transformations:

- $A \rightarrow B$: adiabatic and reversible (isoentropic) compression with increase in pressure and temperature and subsequent decrease in volume;
- $B \rightarrow C$: heat supply at constant pressure (isobar) with increase in volume and

temperature;

- $C \rightarrow D$: adiabatic and reversible (isoentropic) expansion with decreasing pressure and temperature and consequent increase in volume;
- $D \rightarrow A$: heat subtraction at constant pressure (isobar) with decrease in temperature and volume.

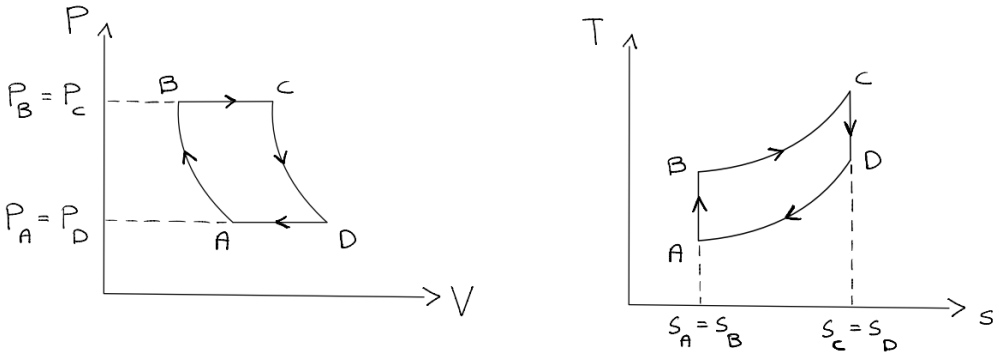

Figure 2.3: Ideal Joule cycle on Gibbs and Clapeyron diagrams

The ideal gas turbine cycle efficiency is calculated as:

$$\eta_{id} = 1 - \frac{1}{\pi^{\frac{\kappa-1}{\kappa}}} \tag{21}$$

2.1.5 Turbine cooling

As can be seen from Eq. 21, the ideal efficiency depends only on the pressure ratio π and the ratio of specific heats κ, but does not depend on the maximum cycle temperature. The efficiency rises as κ rises (i.e. monoatomic gases are the best) and increases towards unity value when the pressure ratio increases towards infinity. This means that also the turbine inlet temperature increases and is good from a thermodynamic point of view, but in the real cycle there are limitations on the pressure ratio because of the materials of which the turbine is made. Indeed, modern gas turbines operate with turbine inlet temperatures higher than the melting temperatures of the super-alloys of which the hot gas path structures are made [3]. For this reason there is a need to cool the engine components exposed to these high temperatures using air bled from the compressor at a higher pressure than the flow to be cooled. This secondary air flow is also useful in balancing the pressure distribution on the rotating discs to keep bearing loads within

acceptable limits [7]. However, this cooling flow decreases the performance of the turbine so it can be understood that the future trend is to develop new materials that can withstand higher temperatures.

Not only must the turbine blade be kept at safe temperatures, but also the wheel space below the hub between stator and rotor discs. This is another function of the secondary air system and occurs through the cavity purge flow, which travels inside the wheel space to exit via the rim seal and mix with the main gas flow, causing further losses that must be minimized. This requires a compromise between wheel space cooling and mass flow used to seal the cavity.

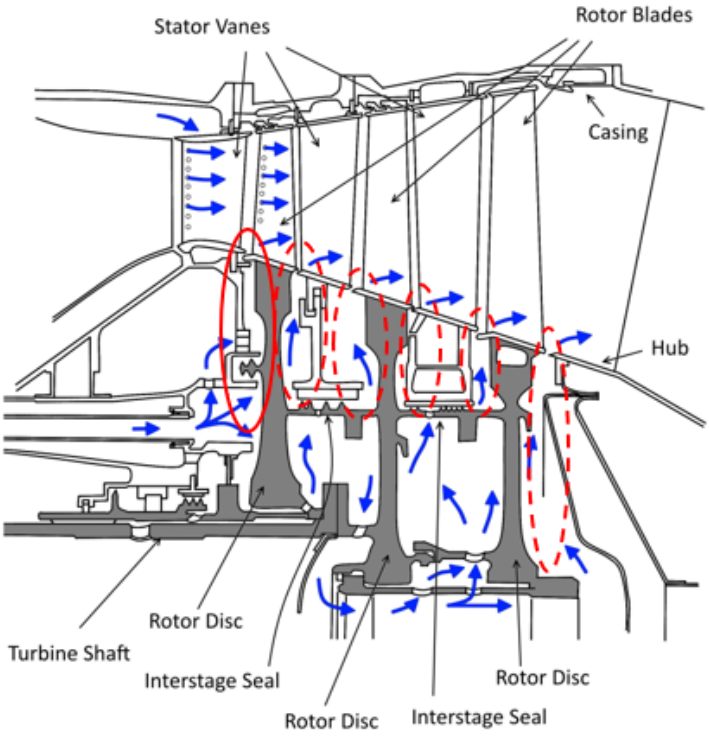

Figure 2.4: Secondary air system of a gas turbine. Adapted from [8]

2.1.6 Loss mechanisms in turbomachines

Any flow characteristic that reduces the efficiency of a turbomachines is called loss and it is defined in terms of entropy increase. The sources of entropy are viscous friction in boundary layers, viscous friction in free shear layers, non-equilibrium processes characterizing shock waves, and heat transfer through finite temperature differences (such as from the main flow to the coolant flow). Although losses have historically been divided into profile loss, secondary (or endwall) loss and tip leakage loss, it is known that the loss

mechanisms are rarely truly independent. Profile loss is generated in the blade boundary layers at a great distance from the end walls. Endwall loss is also referred as secondary loss since it results in part from the secondary flows created by the interaction between the blades and the annulus boundary layers that form along the endwalls. The latter component of loss is the most challenging to predict and, for turbines, is a main source of efficiency loss. Tip leakage loss results from the leakage of flow at the rotor blade tips and stator blade hub clearance, and may have a strong interaction with the endwall loss. However, it is often difficult to separate these three losses and the term secondary loss is sometimes used to cover all losses that cannot be accounted for in any other way [4].

The boundary layer develops near a solid boundary where viscous effects have reduced the velocity below the free-stream value. The fluid velocity changes from zero (at the surface, due to the no-slip condition) to the free-stream velocity of the fluid away from the surface. At low Reynolds number, the boundary layer is laminar; then, at higher Reynolds number, the laminar boundary layer changes to turbulent. Usually, in the boundary layer, the velocity changes most rapidly near the surface, which leads to the majority of entropy generation being concentrated in the inner part of the layer. This is particularly true for turbulent boundary layers, where most of the entropy is produced within the laminar sublayer and the logarithmic region. To quantify the rate of entropy production, a non-dimensional dissipation coefficient is used, which is approximately constant for turbulent boundary layers, while it depends on the thickness of the boundary layer for laminar boundary layers. In the range where both boundary layers exist, the dissipation coefficient in the laminar boundary layer is lower than that in the turbulent boundary layer [4].

Entropy creation due to viscous shear takes place whenever a fluid experiences a shear strain rate. However, the shear strain rate differs from vorticity, meaning that viscous dissipation is not limited to boundary layers. This happens in the so-called free shear layer, also known as mixing layer, which develops between two fluid streams moving at different velocities, thus not necessarily near a surface. This type of shear layer can be observed in scenarios such as jet or nozzle exhausts, mixing ducts within jet engines, sudden flow expansions, and ejectors. It is characterized by a large velocity gradient normal to the layer, meaning there is a rapid change in velocity across the layer . It is rarely possible to accurately quantify the local rates of entropy generation because the flow processes involved are highly complex and often unsteady [4], [9].

Shock waves are irreversible and therefore generate entropy as a result of heat conduction

and the presence of high normal viscous stresses within the shock wave. Shock waves can be normal or oblique, and the latter producing less entropy at the same upstream flow velocity. In turbines, shock waves are generally oblique, even though the local Mach number may be high. The most critical consequence of transonic flow in turbines is the shock system which forms at the trailing edge; the low base pressure that develops just behind the trailing edge can lead to significant trailing edge losses. As the flow expands around the trailing edge to this low pressure, it is then recompressed by a strong shock wave where the flows from the suction and pressure sides converge. In cooled turbine blades with thick trailing edges, this phenomenon may represent the largest single source of loss in the machine. Furthermore, in both compressors and turbines, there can be an interaction of the shock wave with the boudndary layer: the result is the formation of a boundary layer separation bubble at the foot of a weak shock, leading to dissipation within and downstream of the bubble, and therefore additional losses [4].
Heat transfer from a turbomachines to the surrounding environment is a loss. Any heat loss from the compressor must be compensated for by burning additional fuel in the combustion chamber, resulting in a loss of cycle efficiency. As for the turbine, any heat loss reduces the power output. The cooled turbines experience the major effect of heat transfer because the coolant flow is mixed with the main flow and the resulting mixture expands in the other stages, resulting in less work extracted from the main flow. However, it has been found that in cooled turbines, the primary source of this loss is entropy generation due to viscous effects rather than heat transfer. Also, adding coolant to a high Mach number main stream is much more damaging than at low Mach number, and coolant should be injected as parallel to the main stream as possible [4].

2.2 Cavity purge flow

2.2.1 Interaction between purge flow and main annulus flow

The wheel space is a cavity found in gas turbines, located radially below the hub between the rotor and stator. A key objective is to minimize fluid interaction between this cavity and the main annulus. In high-pressure gas turbines, where the main annulus experiences high temperatures, the disc pumping effect can cause a rise in the cavity's temperature. To minimize fluid exchange between the main annulus and the cavity, a rim seal is installed in the hub area. Different seal designs are commonly employed, including radial and axial

clearances, single and double seals, as well as configurations where the seal extends from either the stator or rotor toward the opposite side [3].

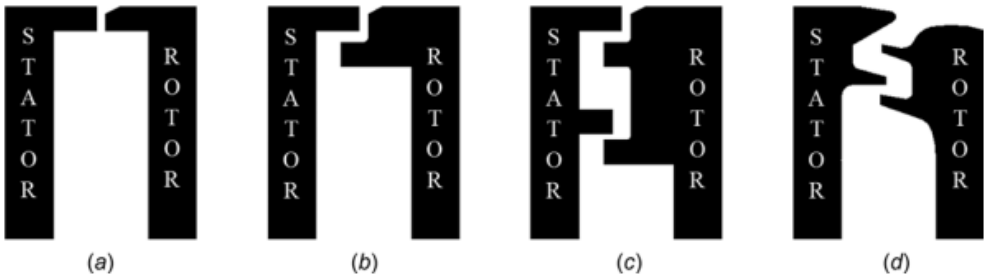

Figure 2.5: Examples of seal geometries: (*a*) axial-clearance, (*b*) radial-clearance, (*c*) double radial-clearance, (*d*) engine-representative double-clearance seal. Adapted from [10]

Flow entering the cavity is called ingress, while flow leaving the cavity is referred to as egress. Basically, the rim seal has a dual purpose: to limit the ingress of flow from the main annulus and to minimize the negative impact of egress on stage performance. Also, to limit the heat transfer from the main annulus to the cavity is possible to use the so called superposed purge flow. This external flow, at a relatively lower temperature, is injected into the cavity, usually near the machine shaft. The purge flow prevents any potentially harmful ingress that could otherwise affect the performance of the turbine, but on the other hand the purge flow exits through the rim seal into the main flow, decreasing turbine efficiency. Indeed, the lower velocity of the cavity flow with respect to the main flow creates a shear mixing between the two streams and so entropy generation. It is important to note that the use of a purge flow is detrimental to performance, regardless of mixing phenomena: the reason is that this flow must be pressurized to a proper level, and to do this it is necessary to sacrifice useful work [3].

2.2.2 Disc pumping effect

Flow through a rotating disc system was first studied by Theodore von Kármán in 1921. With the emergence of gas turbines and the growing interest in the aviation industry during the Second World War, studies on wheel space flow systems became much more detailed [3]. Over the years, many researchers have studied rotating disc flow, flow around rotating cylinders and flow in rotating cavities. Among them, Owen & Rogers [11] provided a comprehensive review of this field, while recently Peter Childs [12] has focused on the so

called *disc pumping effect*, which regulates the flow inside the cavity. This phenomenon is driven by the boundary layer and can be analyzed by observing the flow around a free rotating disc, as illustrated in Figure 2.6.

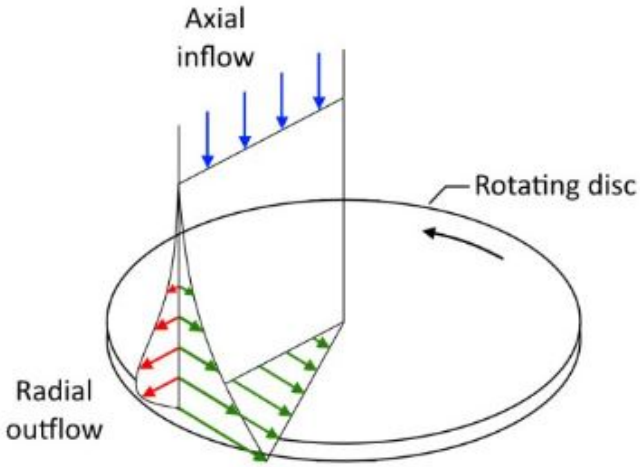

Figure 2.6: Free disc rotating in a surrounding fluid. Adapted from [12]

At the disc surface, the flow is forced to assume the disc velocity because of the no-slip condition. Moving away from the disc in the normal direction, a boundary layer velocity profile develops for the tangential velocity component, since the flow is no more bound to the disc. However, due to the tangential velocity and the fact that the flow is no longer bound to the disc, a radial velocity component also develops as a result of centrifugal effects. Since the flow is leaving the disc radially, an axial inflow is necessary to satisfy the conservation of mass.

2.2.3 Flow regimes in wheel space

Daily & Nece [13] divided the flow regimes within the rotor-stator cavity in terms of rotational Reynolds number and gap ratio. The hub radius b is used as the characteristic length for the rotational Reynolds number:

$$Re_\theta = \frac{\rho \cdot u \cdot b}{\mu} \tag{22}$$

The gap ratio is equal to the axial distance between the rotor and stator discs divided by the hub radius:

$$G = \frac{a}{b} \tag{23}$$

Four regimes were identified in which flow can be either turbulent or laminar, and in both cases boundary layers can be merged or separated. Figure 2.7 shows the map of the possible regimes; each number on the map corresponds to a zone, as below:

1. Laminar flow, small clearance, merged boundary layers
2. Laminar flow, large clearance, separated boundary layers
3. Turbulent flow, small clearance, merged boundary layers
4. Turbulent flow, large clearance, separated boundary layers

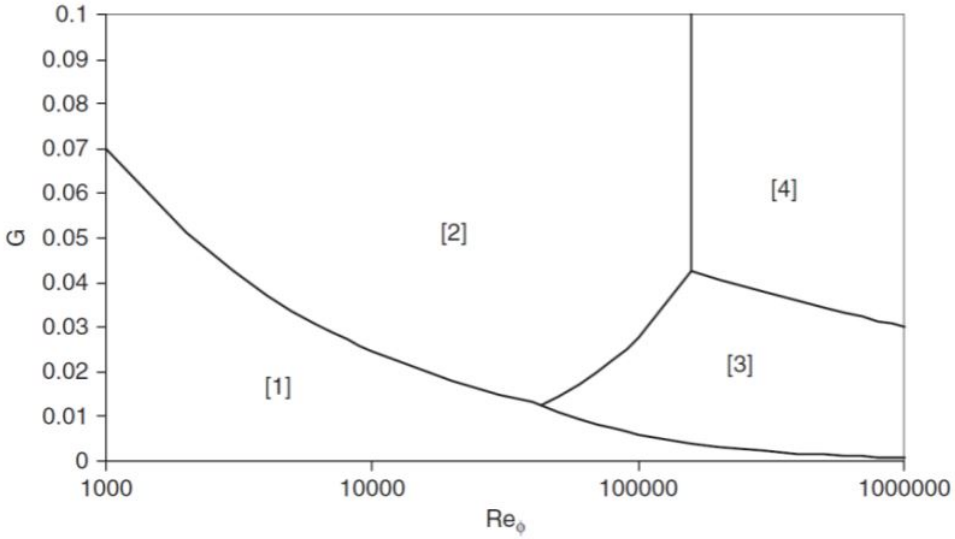

Figure 2.7: Flow regimes of enclosed rotor-stator systems [12]

As far as the thesis project is concerned, the case study refers to zone 4.

2.2.4 Ingestion through turbine rim seals

In a typical high-pressure gas turbine, the flow of gas moving past the vanes and blades in the annulus leads to an unsteady three-dimensional pressure variation radially outward from the rim seal. At the interface between stator hub and rotor hub, in areas where the local pressure is higher than that inside the wheel space, ingress occurs, while in areas where the pressure is lower, egress occurs. This non-axisymmetric type of ingestion is known as *Externally Induced* (EI) ingress [14]. Figure 2.8 shows the potential effect of the leading edge of the blades that creates the tangential pressure variation in the turbine annulus responsible for EI ingress. Red arrows refer to ingress and blue arrows to egress,

respectively marked with '+' and '-' to indicate areas of higher and lower pressure than that in the wheel space.

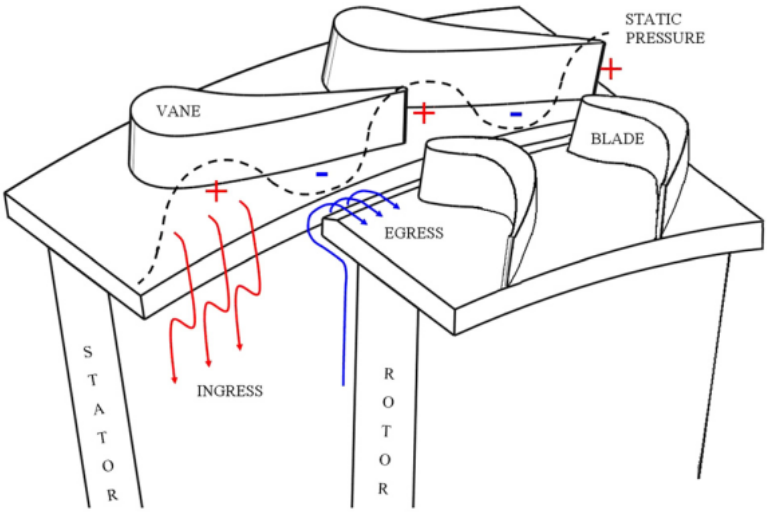

Figure 2.8: *Externally Induced* ingress. Adapted from [7]

Even when the external flow is axisymmetric, i.e. there is no circumferential variation in pressure outside the rim seal, ingress can still occur due to rotational effects. This happens because the rotating fluid within the wheel space generates a radial pressure gradient, causing the pressure inside the wheel space to drop below the mainstream pressure. The *disc pumping effect* creates an outward flow of fluid (egress) near the rotating disc, where the centrifugal effects are greatest. At the same time, to conserve radial mass flow, the lower pressure inside the wheel space causes the main annulus fluid to enter the cavity through the rim seal, close to the stator disc (ingress). This type of ingestion is referred as *Rotationally Induced* (RI) ingress [14] and it is illustrated in Figure 2.9.

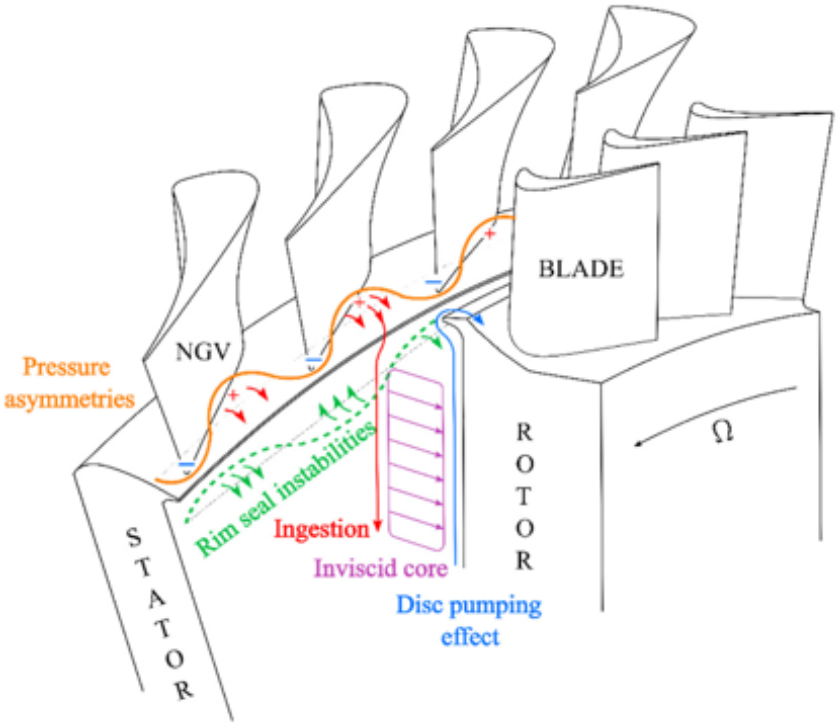

Figure 2.9: *Rotationally Induced* ingress. Adapted from [15]

There are conditions where both EI and RI ingress are of the same order of magnitude: these cases are called *Combined Ingress* (CI). They are common in double rim seals configurations because the circumferential pressure variation in the annular space between the two seals is dampened; if the annular space is large enough to sufficiently attenuate the pressure asymmetry, EI ingress tends to dominate for the outer seal, while RI becomes more significant at the inner seal [14]. Moreover, in off-design conditions, this type of ingestion can play a significant role [10]. However, EI ingress is usually dominant in a turbine.

As stated by Sangan et al. [7], "numerous factors influence the degree of ingestion into the wheel space: the vane and blade geometries and their axial spacing, the Mach and Reynolds numbers of the flow in the annulus, the configuration of the rim seal and its location relative to the vanes and blades, and the non-dimensional sealing flow parameter Φ_o". This last variable is defined in the Nomenclature and will be the subject of further discussion in Section 3.2.

2.2.5 Conceptual flow system in a rotor-stator cavity

Figure 2.10 illustrates the flow structure in a rotor-stator cavity, also showing the superposed purge flow and the ingress/egress through an axial-clearance rim seal. Within the wheel space, separate boundary layers develop on both the rotor and stator. Between these, exists an axisymmetric rotating core of inviscid fluid. Fluid travels axially across the rotating core, moving from the boundary layer on the stator to that on the rotor, thus feeding the rotor boundary layer. The coolant sealing flow enters the wheel space at low radius and is mainly entrained into the rotor boundary layer, providing much more cooling on this side than on the stator side (this is called *rotor buffering effect* and was studied by Mear et al. [16]). The boundary layer on the rotor thickens with increasing radius, while the coolant flow is diluted as it moves towards the higher radius due to the axial flow from the stator to the rotor. In the outer region, part of the coolant flow exits through the rim seal into the turbine annulus, while the other part mixes with the hot gas ingested from the annulus. This mixture is transported into the boundary layer on the stator side, feeding the rotating core. Thus, unlike the rotor boundary layer, the stator boundary layer is thicker at the higher radius and then loses mass as it moves inward into the cavity. As the non-dimensional sealing flow rate increases to Φ_{min}, which is the minimum value of Φ_o to prevent ingress, the core region is reduced and pushed to a higher radius [3], [7].

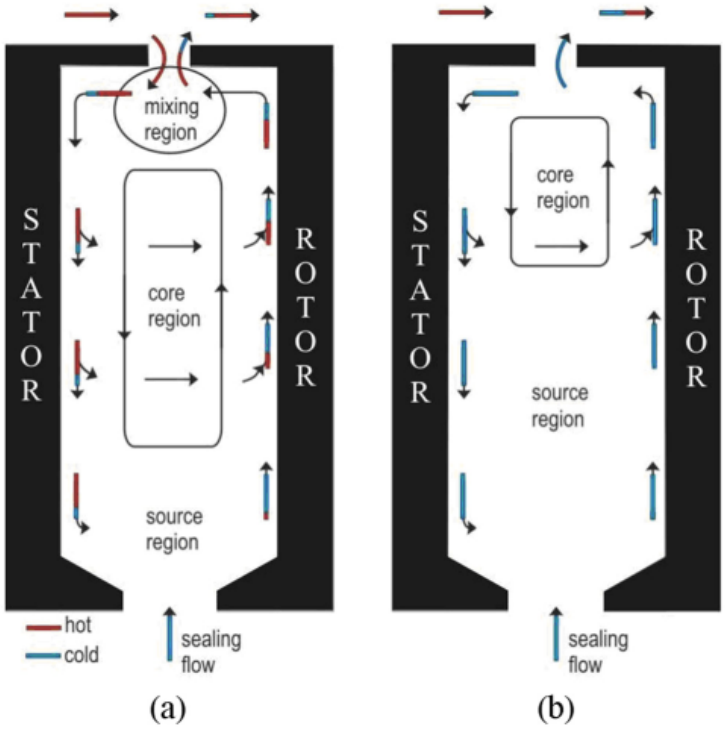

Figure 2.10: Flow structure inside the wheel space: (a) $\Phi_o < \Phi_{min}$, (b) $\Phi_o = \Phi_{min}$. Adapted from [7].

The fluid dynamics in the cavity boundary layers can be understood using the mass-transfer analogy. Please note that in this section c does not refer to the absolute flow velocity as defined in the Nomenclature. Referring to Figure 2.11, consider the case where a tracer gas with a concentration $c_0 = 1$ is added to the purge flow, while the concentration in the annulus is zero. Since no fluid is entrained by the stator boundary layer as it travels inward in the cavity, the concentration remains constant on the stator side. This implies that if the fluid in the stator boundary layer is fully mixed, then the concentration at the stator side (c_s) should be equal to the concentration in the inviscid core at the boundary layer's edge (c_∞). As the fluid exiting the stator boundary layer travels axially across the rotating core, the concentration of the fluid in the rotor boundary layer is $c_\infty = c_s$. The tracer gas then diffuses through the rotor boundary layer, resulting in a concentration at the rotor surface c_r that is greater than $c_\infty = c_s$. This represents the mass-transfer analogy of the *thermal buffering effect*. Since $c_r > c_s$, the coolant flow mitigates the impact of hot-gas ingestion on the rotor. As the fluid moves radially outward, entrainment into the boundary layer causes c_r to decrease. The concentration on the rotor should be constant with radius in the outer region, as the fluid moves away from the rotor boundary

layer. An engine would also have its rotor disc temperature affected by friction heating and conduction, which the buffering model does not take into account [10].

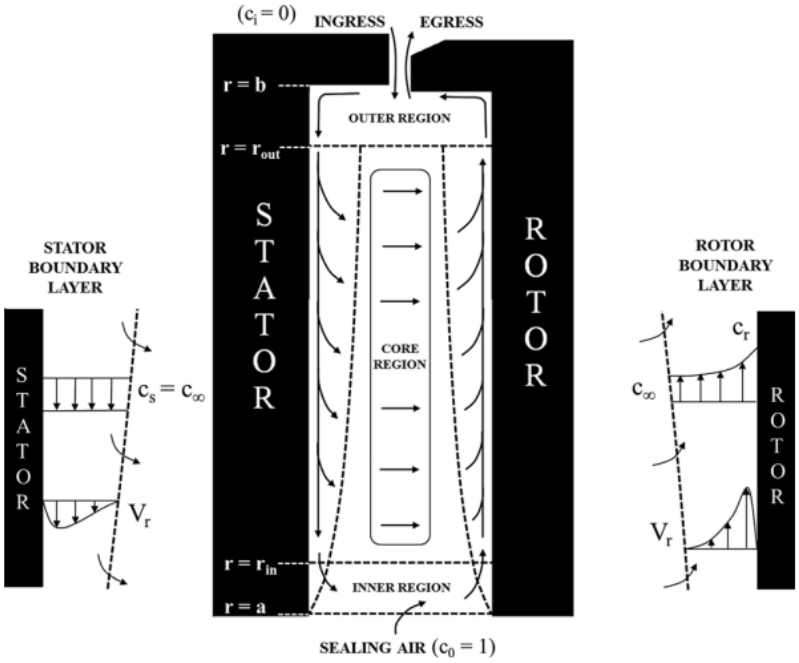

Figure 2.11: Simplified flow structure for system with superposed sealing flow and ingress. Side plots show radial velocity and concentration profiles within the boundary layers [10]

Depending on the gap ratio, defined as the ratio of the axial distance between the stator and rotor disc over the hub radius, the inviscid core can develop or not. If the inviscid core exists, the flow inside the wheel space behaves according to the *disc pumping effect* and this case is referred as separated boundary layer. The opposite is true for a narrow cavity, in which the boundary layers on the stator and rotor merge so that there is no inviscid core. Figure 2.12 shows the velocity components for both cases. The inviscid core is characterized by a tangential velocity plateau and zero radial velocity (according to the Taylor-Proudman theorem [11], an axisymmetric inviscid rotating core cannot have axial gradients of the tangential and axial velocity components, and the radial one should be zero). Instead, in a narrow cavity, there is a continuous gradient of tangential velocity through the whole axial space, and the radial velocity passes zero only at the transition from radial inflow on the stator side to outflow on the rotor side, near the cavity centre. Please note that the velocity components in the Figure 2.12 are not scaled. The actual relationship is $v_\theta > v_r > v_x$, where the tangential velocity is significantly greater than the axial one, often differing by several orders of magnitude [17].

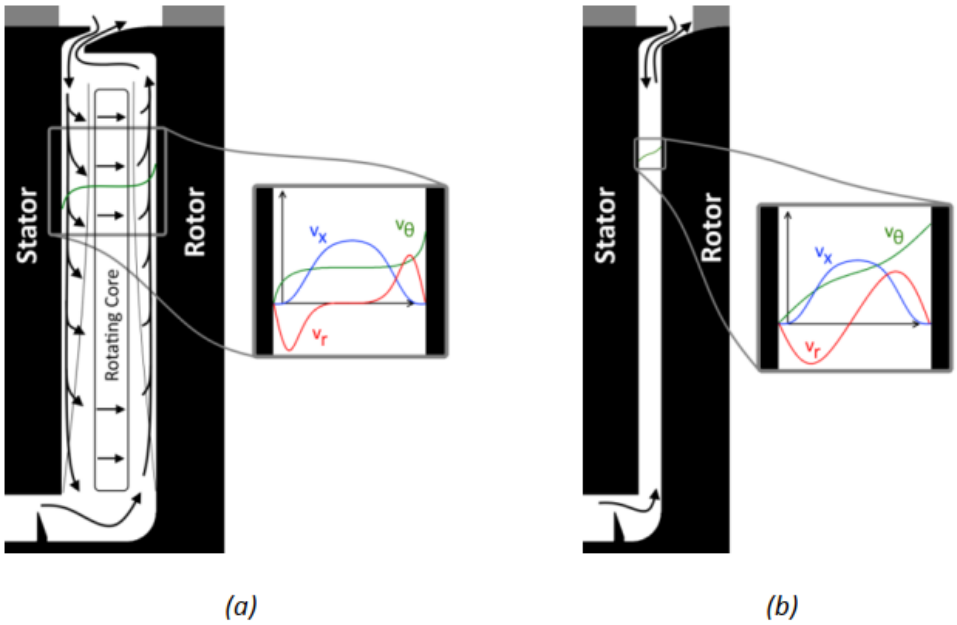

Figure 2.12: Schematic flow system of rotor-stator cavity with separate (a) and merged (b) boundary layers [3]

2.2.6 Swirl ratio

An important parameter in cavity flow analysis is the swirl ratio β, defined as the ratio of the tangential velocity of the fluid in the wheel space to the tangential velocity of the rotor.

$$\beta = \frac{\omega}{\Omega} = \frac{c_\theta}{\Omega \cdot r} \tag{24}$$

The gap ratios studied in test rig turbines subjected to the cavity flow study are typically of separated boundary layer. In flow regimes of separated boundary layers, a rotating inviscid core exists, characterized by a constant angular velocity ω and thus by a constant swirl ratio across radius. In turbine applications, the wheel space system features ingress and egress flows that change the swirl ratio due to the angular momentum with which they enter the system. In this regard, Facchini et al. [18] develpoed an empirical correlation based on the swirl ratio of a cavity with no net mass flow, taking into account a corrected radial position and the turbulent flow parameter λ_t (as the wheel space flow is predominantly turbulent) [3].

2.2.7 Interaction between purge flow and secondary flows

Secondary flows refer to flow structures that diverge from the expected behavior. Among them, the most significant are the passage vortex, the horseshoe vortex and the tip leakage vortex. The passage vortex is generated by the behavior of the boundary layer in a curved vane. Fluid near the endwalls moves to the suction side of the blade, while fluid near the mid-span is transported to the pressure side [19].

Horseshoe vortices are formed at blade leading edges of the stator and rotor blades, near the hub and tip endwalls. As for trailing edge, wakes develop and are dissipated downstream to be conveyed with the main flow into the next cascades [20]. Horseshoe vortices are two counter-rotating vortices formed by the stagnation line in the boundary layer zone, which move inside of two adjacent vanes towards the blade suction sides and can interact with the passage vortices [19].

Tip leakage vortex results from the small percentage of the flow passing from the pressure to the suction side of the blade via the gap between the blade tip and the casing (the so-called tip-gap). This phenomenon can be observed in Figure 2.14. Tip leakage vortex is counter-rotating to the passage vortex at the blade tip (see Figure 2.13) and, also, may have a higher intensity that forces the passage vortex to move toward mid-span. As can be seen from Figure 2.13, the tip leakage vortex is one of the most important sources of entropy generation, and thus losses, in transonic turbine stages [19].

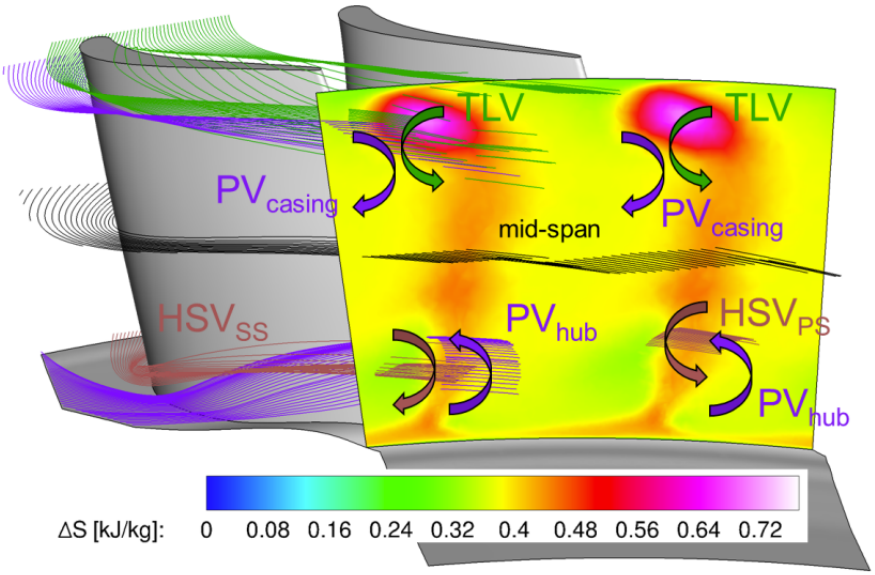

Figure 2.13: Secondary flow visualization in a turbine blade [19]

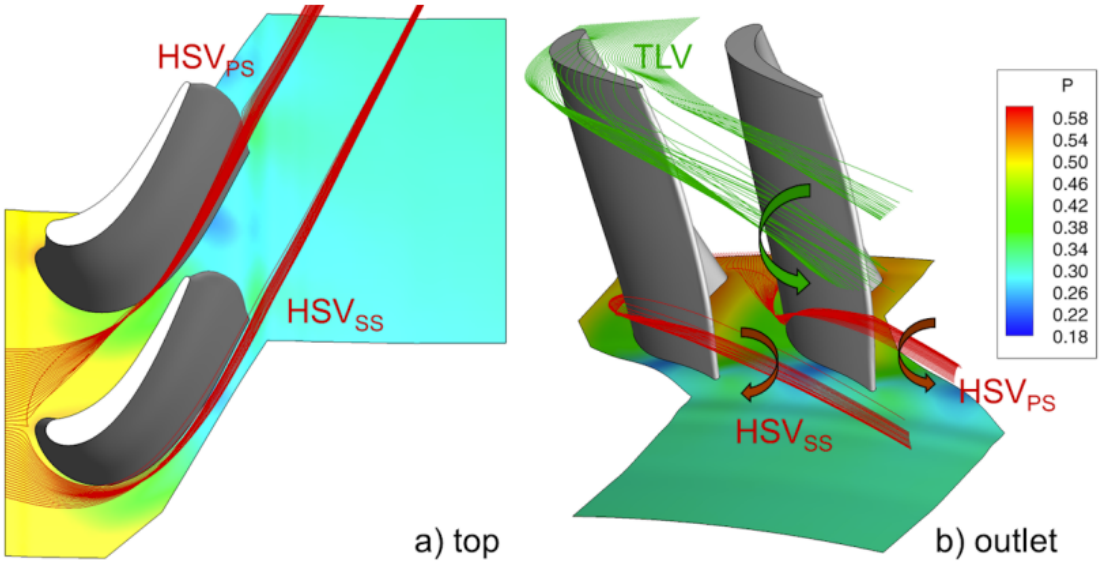

Figure 2.14: Visualization of the horseshoe vortex and of the tip leakage vortex in a high-pressure turbine blade along with the non-dimensional static pressure map on the lower endwall [19]

The secondary flows generates a reduction in stagnation pressure and an increase in overall losses [4], so it is essential to evaluate them to calculate the performance of the turbine. Furthermore, these flows influence the heat transfer and film cooling performance of the endwall by interacting with the purge flow. Burd et al. [21], [22] showed that a higher purge flow rate prevents coolant from being drawn into the secondary flow and ensures effective cooling at the endwall. Rehder & Dannhauer [23] demonstrated that purge flow ejection perpendicular to the main flow direction enhances both the horseshoe vortex and the passage vortex, especially in the region between the gap and the vane leading edge, leading to an increase in heat transfer on the endwall; on the contrary, the tangential ejection considerably weakens these secondary flows, reducing their impact on the heat transfer. Ong et al. [24] found that the cavity flow is entrained into the secondary flow of the rotor hub and the negative incidence of the cavity flow reinforces the secondary flow and enhances its penetration depth.

Song et al. [25] analyzed the effect of purge flow on endwall film cooling, heat transfer characteristics and aerodynamic losses of a gas turbine blade, for different mass flow ratios of the purge flow and different ejection angles α (please note that in this section α is not the absolute flow angle related to the velocity triangles as defined in the Nomenclature). The high film cooling effectiveness region is restricted to the fore part of the passage

near the suction side since the secondary vortices near the endwall sweep the coolant ejection (i.e. the purge flow) toward the suction side. This means that it is difficult for the coolant to cover the pressure side. Moreover, the horseshoe vortex can roll down the mainstream flow to improve the mixing between the main flow and the coolant to reduce the film cooling effectiveness around the leading edge. Increasing the MFR, the purge flow improves the film cooling effectiveness on the endwall because the coolant has larger momentum to overcome the effect of the secondary vortices. The effect of the ejection angle α is manifested as the MFR increases, and as the ejection angle increases, the effectiveness of the film cooling on the endwall decreases. However, the purge flow can increase the horseshoe vortex intensity and cause the separation of the incoming boundary layer to form separation vortex. As the MFR and α increase, the heat transfer coefficient of the endwall is enhanced but this is not good for cooling protection of the endwall.
The purge flow has two opposite effects on the passage vortex. On the one side, the cavity flow can increase the horseshoe vortex; the pressure side leg of the horseshoe vortex moves toward the suction side because of the normal pressure gradient between pressure and suction side and interacts with the lower branch of the passage vortex (that has the same direction of rotation, as shown in Figure 2.13) to strengthen the passage vortex intensity. But the purge flow can also raise the momentum of the boundary layer which allows the fluid in the boundary layer to resist the normal pressure difference between the pressure side and the suction side, thus reducing the intensity of the passage vortex [19]. From the studies conducted by Song et al. [25], it was found that the purge flow increases the aerodynamic losses with respect to the case without purge flow, as shown in Figure 2.15. When $\alpha > 45^o$, the improvement of the boundary layer momentum by the purge flow is not significant, so the purge flow can strengthen the passage vortex intensity and this results in an increase in aerodynamic losses as the MFR rises. When $\alpha < 45^o$ and $MFR < 1\%$, the purge flow does not affect the momentum of the boundary layer, so the intensity of the passage vortex grows and consequently the aerodynamic losses. When $\alpha < 45^o$ and $MFR > 1\%$, the purge flow improves the momentum of the boundary layer reducing the intensity of the passage vortex and thus the aerodynamic losses.

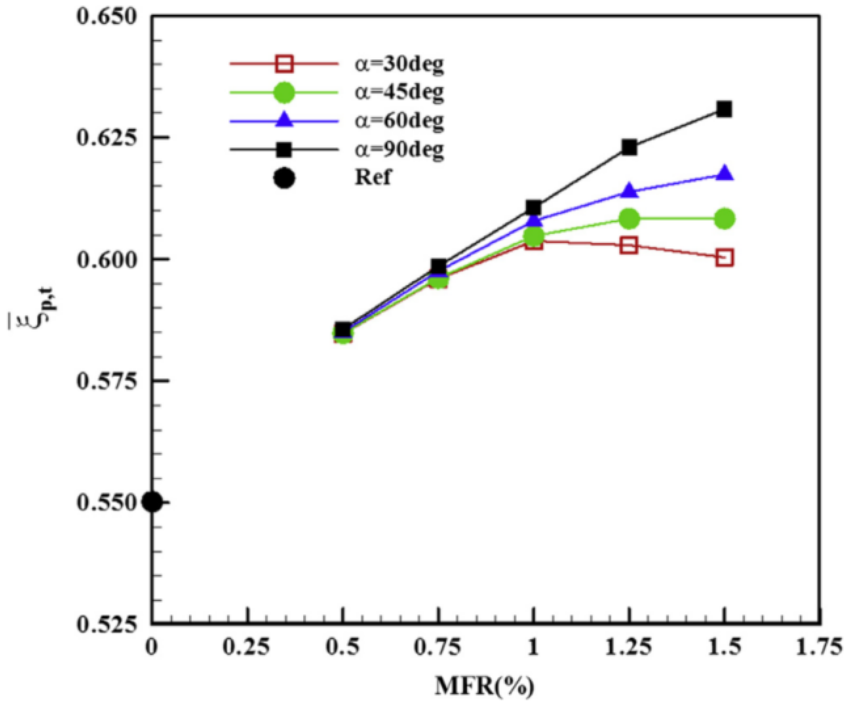

Figure 2.15: Total pressure loss coefficient for different MFR and ejection angles α [25]

3 Methodology

All data acquired during the thesis project were collected through the Test Turbine of the Energy Department at KTH. This section describes the test rig, its data acquisition instrumentation, the methods used to compute the data, the experimental procedure and the operating points tested.

3.1 Experimental facility

The Test Turbine is a joint venture between KTH and Siemens Industrial Turbomachinery (Finspång) started in early 1990's. Research have centered around aerodynamic stage/cascade efficiencies/losses at engine representative velocities. Certain focus area have been or are studied: airfoil/stage design, axisymmetric endwall contouring, partial admission, cavity purge flow characterization, trace gas measurements, aero/heat transfer (steady/unsteady), turbulence intensity study, tip gap study, hub enwdall flows. In 2012 the focus shifted from mainly steam turbine research to gas turbine research.
With regard to the cavity purge flow studies, the purpose and objectives of the Test Turbine are as follows [26]:

- understand the effect of varying cavity purge flow rate on the turbine aerodynamic performance;
- use seedgas sampling to trace the mixing between purge flow and main annulus flow and validate with CFD predictions;
- understand the radially flow variation to verify the presence of ingress/egress areas and validate with CFD predictions;
- visualize the change in flow structures within the cavity as the purge flow rates and Reynolds number change. Also try to identify the instabilities and find an optimum flow rate to avoid instabilities;
- understand the effect of changing the pressure ratio across the stage on the purge mixing and flow behaviour. In addition, perform unsteady analysis of the purge mixing and rotor wake to identify frequencies of instabilities and their sub-harmonics, particularly in relation to tip vortices and leakage flow from rotor tip gap;

- validate the results with findings from the University of Bath, which has an identical test rig, and then run the same experiments at higher turbine operating points.

The results so far are as follows [26]:

- global performance analysis has identified the maximum efficiencies that can be achieved at the design operating conditions and the parameters that can contribute to further improvements;
- concentration measurements showed similar behaviour to the University of Bath results at high radial positions, but low radial positions have a slightly different flow phenomenon, which will be analyzed;
- steady initial CFD simulations show a similar behaviour to the experimental data, but the torque is a little undermined, which is also under investigation and improvement.

3.1.1 Background

Originally described by [27], the rig is an open-cycle testing facility that allows the study of turbine stages in a rotating environment. The air supply in the laboratory comes from a broad spectrum of available compressors and fans, chosen according to the experiment in question (low speed, high speed) and the flow and pressure requirements. For the Test Turbine, the air is provided by a 1 MW screw compressor with a maximum pressure of 4 bar, a maximum mass flow of 4.7 kg/s and a temperature range of 30°C to 90°C. The air passes through a cooler, a condensate water separator, mass flow orifice and a settling chamber before entering the turbine. It is possible to test up to three stages of the turbine, but the configuration currently installed is single stage and the thesis project was carried out on this [28]. Figure 3.1 shows an overview of the assembled facility, highlighting the inlet, the purge inflow with all the pressure taps, the test section and the outlet. The turbine output power is measured by a torquemeter mounted on the output shaft and based on the phase shift between the two ends of a carefully calibrated torsion shaft. The turbine speed is controlled by a hydrokinetic dynamometer with variable filling, called water brake, which also has the function of dissipating the power generated in the turbine. Both the torquemeter and the water brake are not highlighted in Figure 3.1 as they are located at the rear of the test rig.

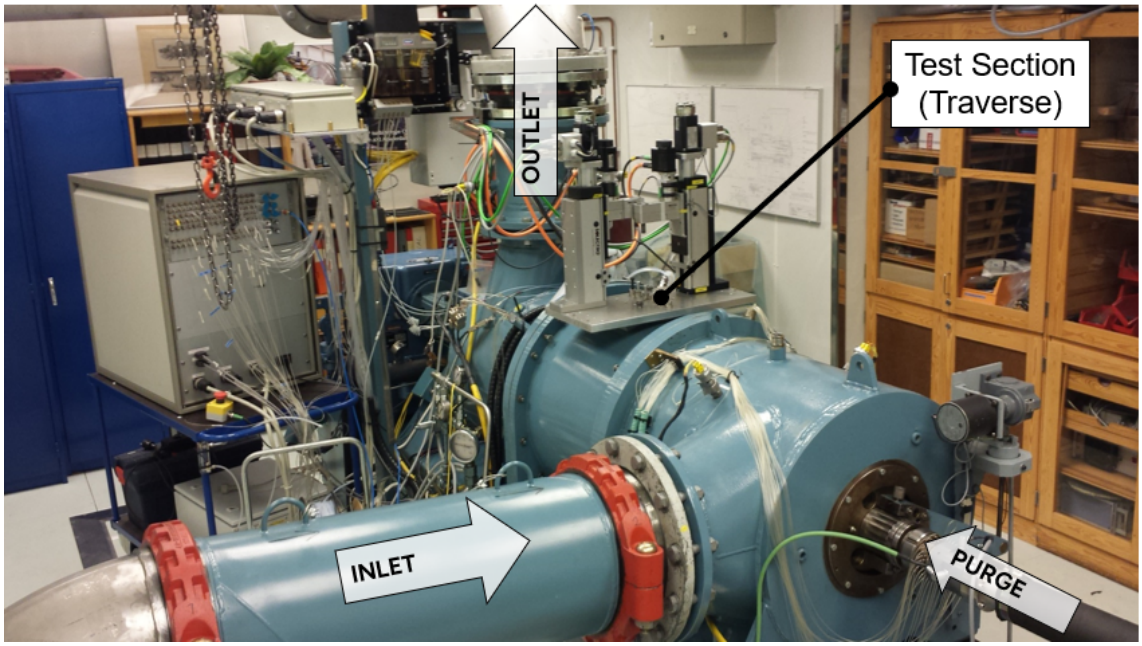

Figure 3.1: KTH Test Turbine

In 2013, the test turbine shaft spindle was upgraded and the existing torquemeter was rebuilt to 13000 rpm, more appropriate for the scaled gas turbine stages now being investigated. This update had a problem with high vibrations and it has severely restricted the permissible speeds in the operating envelope, especially at high speeds between 9,000 and 13,000 rpm, where the design point for the relevant stages of scaled gas turbines is located. It was therefore decided to invest in a new torquemeter in 2023, with the aim of reaching up to 15,000 rpm and mapping vibrations to determine the permissible operating envelope. Not only has this goal been achieved, but the possible points of operation where measurements can be made safely have been greatly expanded [29].

3.1.2 Test Turbine layout

The aerodynamic characteristics of the rotor and stator disc are to scale with a typical high pressure gas turbine stage. The aerodynamic design was done by Siemens Energy AB [28] and the structural design by KTH [30]. Some turbine components, such as the stator (42 vanes), have remained the same over time, while other instrumentation have only been upgraded. The rotor disc (also referred to as Blisk, Build or Obj.) has been modified over time: the version mounted during the thesis project was the Blisk 6, which differs from the previous Blisk 5 in having a reduced number of blades, 49 and 60 respectively, while maintaining the same degree of reaction, pressure ratio and material

(Al 7050-T7452). This should improve performance and reduce aerodynamic losses, as high levels of entropy are generated near the blade surface. Also, a reduction in the number of blades reduces the cooling flow rate and manufacturing costs. For example, in a real engine using film cooling, reducing the number of blades could result in a reduction in film cooling flow rate and cost. In addition, to reduce endwall aerodynamic losses and improve performance, a endwall contouring has been applied to the Blisk, resulting in a pronounced non-axisymmetric hub. Figure 3.2 shows a cross section of the stator and rotor, illustrating the non-axisymmetric shape of the rotor hub, while Figure 3.3 shows the Blisk 6.

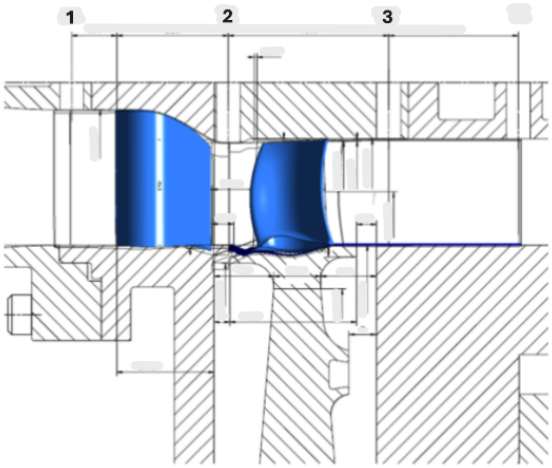

Figure 3.2: Cross section of the Test Turbine, showing the stator and rotor

Figure 3.3: Rotor Blisk 6

The Table 3.1 gives some geometric stage parameters and main stage characteristics at the design point. Unless otherwise stated, the parameters are given at midspan. Please note that the Table 3.1 uses the same nomenclature as [29], so it is not the same Nomenclature used in this report.

Table 3.1: Selected geometrical and design point parameters [29].

	Build 5		**Build 6**	
Parameter:	**stator**	**rotor**	**stator**	**rotor**
Hub radius r_h [mm]	177.5	177.5	177.5	177.5
Diameter ratio, TE, d_h/d_t [-]	1.149	1.148	1.149	1.149
Pitch-chord ratio, t/b [-]	0.83	0.84	0.83	1.08
Aspect ratio, TE, h/b [-]	0.77	1.10	0.77	1.16
# of blades	42	60	42	49
tip clearance [mm]	-	0.4	-	0.4
Flow turning, γ_{mid} [°]	75.3	106	75.3	
Rotational speed [rpm]	-	10300	-	10500
Mach number $Ma_{exit,rel}$ [-]	0.779	0.782	0.779	
Reynolds number Re_{rel} [-]	$6.9 \cdot 10^5$	$3.7 \cdot 10^5$	$6.9 \cdot 10^5$	
Mass flow [kg/s]	3.47		3.49	
Pressure ratio, Π_{t-s} [-]	2.139		2.139	
Pressure based reaction degree, $\Lambda_{p,mid}$ [-]	0.389		0.389	
Flow coefficient, ϕ [-]	0.423		$0.54_{mid,TE}$	
Stage loading coefficient, ψ [-]	1.368		1.30_{mid}	

3.1.3 Instrumentation setup

Stationary operating conditions are measured by static and total pressure taps and static and total temperature taps, called fixed instrumentation. The measurements are sent digitally to a PC running LabView, which is used to monitor and aggregate the data into a single output file. It is possible to combine fixed instrumentation measurements with detailed flow field investigations. These investigations are mainly carried out using pneumatic probe traverses. The traverse locations are positioned both upstream and downstream of the rotor and stator. 5-hole conical probes are used to determine the flow characteristics and loss distributions in each section. The Traverse can be used to quantify the concentration of the purge flow in the main annulus after the rotor using seedgas concentration measurements. This allows the mixing process to be quantified in the axial

direction and the effect on flow phenomena to be linked to the presence of purge flow. A Rosemount NGA 2000 MLT gas analyzer is used for seedgas sampling, based on infra-red detection for gas identification. The analyzer was calibrated using N_2 as zero-gas and a mixture of 8000 ppm CO_2 mixed with N_2 as span-gas [31].

The purge flow passes radially through the constant width cavity via the lower labyrinth seal on the rotating shaft. A radial rim seal is mounted in the hub area of the cavity. As far as cavity purge investigations, static pressure taps are installed in the wheel space upstream of the rotor, on the stator side, in both radial and tangential directions. The purpose of the radial static pressure taps is to quantify the swirl ratio, directly related to RI ingress. The circumferentially distributed taps are placed after the trailing edge of the vanes, along one vane pitch, to quantify the tangential pressure variation in the main annulus flow, which is the main driving force for EI ingress [31]. The magnitude of such a driving force can then be evaluated through the hub non-dimensional pressure difference ΔC_p (also called pressure coefficient):

$$\Delta C_p = \frac{\Delta p}{\frac{1}{2} \cdot \rho \cdot \Omega^2 \cdot b^2} \tag{25}$$

Δp is the so-called peak-to-trough difference in static pressure in the annulus, i.e. the maximum tangential pressure difference on the hub (above the rim seal). The latter can also be evaluated at the highest measurement location inside the cavity (below the rim seal) to obtain the cavity pressure coefficient and compare it with the corresponding value on the hub. This is useful for identifying where ingress is most prone to occur along the vane pitch.

Like the static pressure taps, total temperature thermocouples are installed radially and tangentially in the wheel space.

3.2 Non-dimensional coefficients

Below are some useful non-dimensional coefficients for cavity flow analysis. Look at the Nomenclature for unknown parameters.

Non-dimensional flow rate:

$$C_w = \frac{\dot{m}}{\mu \cdot b} \tag{26}$$

Seal clearance ratio:

$$G_s = \frac{s}{b} \tag{27}$$

Remembering that the rotor blade speed at the hub is defined as $u = \Omega \cdot b$, the rotational Reynolds number, already defined in Eq. 22, can also be expressed as:

$$Re_\theta = \frac{\rho \cdot \Omega \cdot b^2}{\mu} \tag{28}$$

Non-dimensional sealing parameter:

$$\Phi = \frac{C_w}{2 \cdot \pi \cdot G_s \cdot Re_\theta} = \frac{\dot{m}}{2 \cdot \pi \cdot \rho \cdot \Omega \cdot s \cdot b^2} \tag{29}$$

Mean purge flow velocity through the rim seal:

$$U = \frac{\dot{m}}{2 \cdot \pi \cdot \rho \cdot b \cdot s} \tag{30}$$

The latter allows an alternative way for Eq. 29:

$$\Phi = \frac{U}{\Omega \cdot b} \tag{31}$$

Axial Reynolds number in annulus:

$$Re_{c_x} = \frac{\rho \cdot c_{1_x} \cdot b}{\mu} \tag{32}$$

Flow coefficient:

$$C_f = \frac{Re_{c_x}}{Re_\theta} \tag{33}$$

Non-dimensional flow rate (C_w) and non-dimensional sealing parameter (Φ) can be used with the subscripts *i* and *o*, referring to ingress and purge flows respectively. In addition, the Φ coefficient is very important in cavity flow theory since it is useful in reproducing results for scaled geometries and different operating speeds [10].

3.3 Sealing effectiveness

The ingestion behaviour can be experimentally quantified through seedgas measurements by tracking the purge flow with a non-reacting foreign gas (e.g. carbon dioxide), as seen in the following equation:

$$\varepsilon = \frac{\gamma_s - \gamma_{inlet}}{\gamma_o - \gamma_{inlet}} \tag{34}$$

The seedgas concentration (γ) is measured at several locations, as explained below:

- γ_s refers to the radial locations within the cavity;
- γ_{inlet} is the ambient seedgas concentration;
- γ_o is the seedgas concentration at the purge flow inlet.

In order to quantify the performance of the seal, it is common practice to measure the seedgas concentration at different radial locations within the cavity to obtain multiple values of sealing effectiveness. The same values could be derived by the ratio of the purge mass flow rate to the egress mass flow rate, as well as in non-dimensional coefficients:

$$\varepsilon = 1 - \frac{\Phi_i}{\Phi_e} = \frac{\Phi_o}{\Phi_e} = \frac{\Phi_o}{\Phi_o + \Phi_i} \tag{35}$$

Note that from the continuity equation $\Phi_o = \Phi_e - \Phi_i$.
Φ_{min} is the minimum value of Φ to prevent ingress, i.e. the pressure inside the cavity is equal to the maximum hub pressure in the tangential distribution:

$$\Phi_{min} = \frac{U_{min}}{\Omega \cdot b} = \frac{C_{w,min}}{2 \cdot \pi \cdot G_s \cdot Re_\theta} \tag{36}$$

This implies that when $\Phi_o = \Phi_{min}$, the cavity is sealed by the purge flow and $\varepsilon = 1$. The opposite occurs when $\Phi_o = 0$, meaning that no purge is flowing and the cavity is filled by the main annulus flow, resulting in $\varepsilon = 0$ [14].

3.4 Efficiency

As mentioned in Section 2.1.3, the efficiency of a turbine is defined as the ratio between the real enthalpy change of the stage and the ideal isoentropic enthalpy change of the stage. There are two definitions of efficiency, which differ in the isoentropic part:

$$\eta_{tot-tot} = \frac{W}{W_{is_{tot-tot}}} = \frac{h_{01} - h_{03}}{(h_{01} - h_{03})_{is}}$$

$$\eta_{tot-stat} = \frac{W}{W_{is_{tot-stat}}} = \frac{h_{01} - h_{03}}{(h_{01} - h_{3})_{is}}$$

As regards the real enthalpy change, to achieve more general results, it's important to separate the enthalpy change from the torque measured at the turbine shaft. If the output power is based only on the available torque, the overall efficiency would be influenced by mechanical losses specific to the test rig, making the results less applicable in general.

Therefore, torque losses should be either measured or estimated and added to the shaft torque to properly quantify the useful work done by the gas on the turbine blades. This is reflected in the following equation:

$$h_{01} - h_{03} = \frac{\Omega \cdot (\tau_{shaft} + \tau_{losses})}{\dot{m}_{main} + \dot{m}_{purge}} \tag{37}$$

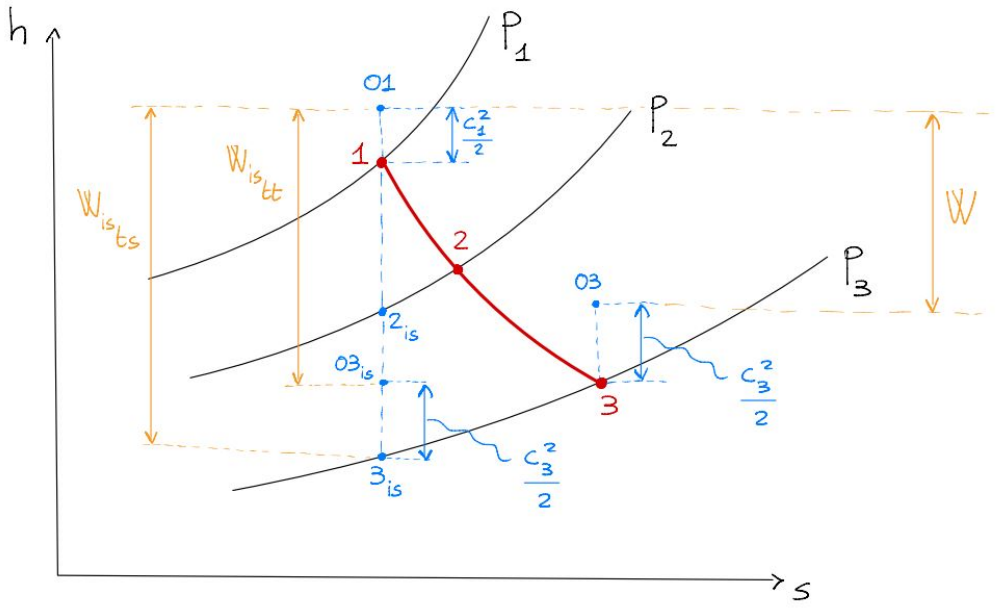

Figure 3.4: h-s diagram for a turbine stage

As for the isoentropic enthalpy change, it can be calculated by applying the first principle of thermodynamics to the turbine stage, assuming adiabatic flow. Looking at Figure 3.4 and remembering the two definitions given in Section 2.1.3, the following equations are obtained:

- total-to-total ($c_3 \neq 0$)

$$Q - W_{is_{tot-tot}} = \Delta h + \Delta e_c \Rightarrow W_{is_{tot-tot}} = h_1 - h_{3_{is}} + \frac{c_1^2}{2} - \frac{c_3^2}{2} = h_{01} - \left(h_{3_{is}} + \frac{c_3^2}{2} \right) \tag{38}$$

- total-to-static ($c_3 = 0$)

$$Q - W_{is_{tot-stat}} = \Delta h + \Delta e_c \Rightarrow W_{is_{tot-stat}} = h_1 - h_{3_{is}} + \frac{c_1^2}{2} = h_{01} - h_{3_{is}} \tag{39}$$

It can be noted that:

$$W_{is_{tot-stat}} > W_{is_{tot-tot}} \Rightarrow \eta_{is_{tot-stat}} < \eta_{is_{tot-tot}}$$

3.5 Orifice Model

The Orifice Model provides a simple way to analyze the ingress and egress problem. It has been derived for both compressible and incompressible swirling flows. The description of the model is rather complicated, so the reader is referred to [32] for RI ingress and [14] for EI and CI ingress, if interested. However, the resulting simple analytical results provide a correlation between the sealing effectiveness and the important parameters of cavity flow theory. It is therefore a simple but very powerful model for predicting ingestion into the cavity. If experimental data are available, it is also possible to check whether the model solution is in good agreement with them.

The Orifice Model is based on an imaginary orifice ring, as shown in Figure 3.5 for an axial-clearance seal. Via the elementary areas δA_e and δA_i, the sum of which is equal to the clearance area of the seal, the egress and ingress simultaneously pass through different parts of the orifice ring. Egress flows through a stream tube in the cavity where the static pressure is p_1 and exits in the external annulus where the static pressure is p_2. Instead, ingress starts in the annulus and exits in the wheel space [14]. Note that, in this section, subscripts 1 and 2 differ from those defined in the Nomenclature.

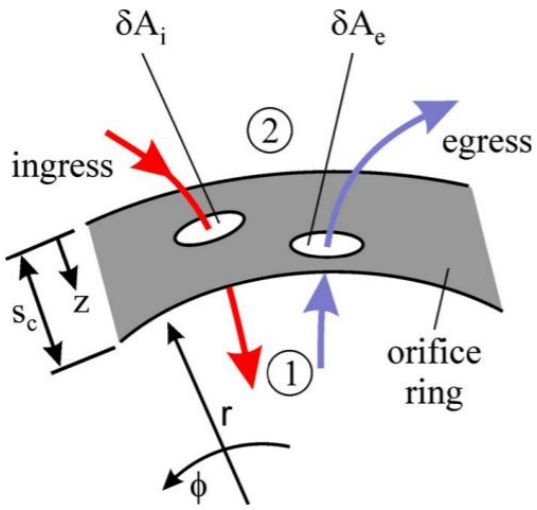

Figure 3.5: Orifice ring. Adapted from [14]

Although the equations are derived for inviscid flow, empirically determined discharge coefficients for egress and ingress ($C_{d,e}$ and $C_{d,i}$) are introduced to take viscous losses into account. Owen's derivation [14] was based on an axial-clearance seal, but it can be adapted to any seal geometry by empirically determining the discharge coefficients (theory cannot predict adequate discharge coefficients).

The advantage of this model is that the equations can be solved analytically for incompressible cases, giving simple results to examine the ingress problem (both EI, RI and CI), which can be used to extrapolate results from the test rig to the real engine conditions. However, real engine turbines operate at large subsonic Mach numbers, where the incompressibility assumption is no longer valid. In the latter case, the equations can only be solved numerically [14].

As far as the thesis project is concerned, only EI ingress was analyzed since it is usually in a turbine. In this case, the solution of the Orifice Model proposed by Owen [14] is the following:

$$\frac{\Phi_o}{\Phi_{min,EI}} = \frac{\varepsilon}{\left[1 + \Gamma_c^{-\frac{2}{3}} \cdot (1-\varepsilon)^{\frac{2}{3}}\right]^{\frac{3}{2}}} \tag{40}$$

Φ_{min} and Γ_c have to be treated as empirical constants.

Φ_{min} has already been defined in Sec. 3.3. For EI, the incompressible orifice equations have been solved analytically by Owen [14] using the so-called "saw-tooth model" to represent the circumferential distribution of pressure in the annulus, resulting in the following expression:

$$\Phi_{min,EI} = \frac{2}{3} \cdot C_{d,e} \cdot \sqrt{\Delta C_p} \tag{41}$$

Γ_c is the ratio of the discharge coefficients, defined as follows:

$$\Gamma_c = \frac{C_{d,i}}{C_{d,e}} \tag{42}$$

From the Eq. 40, it can be seen that the Orifice Model can be used to predict Φ_{min}, the minimum non-dimensional sealing parameter to prevent ingress, from the steady experimental data in terms of (ε,Φ_o) without any knowledge of the annulus pressure distribution and discharge coefficients. Furthermore, the EI ingress is a consequence of the tangential pressure variation in the main annulus, which is an unsteady three-dimensional phenomenon; thus, the Orifice Model is useful to correlate the experimental data by decoupling the cause (hub non-dimensional pressure difference ΔC_p) from the

effect (ingress affecting the sealing effectiveness ε), as this cause and effect relationship is difficult to establish and it is not always possible in an experiment to isolate the many interconnected mechanisms governing ingress [7].
The Orifice Model proposed by Owen does not take into account the impact of the density difference between main annulus flow and purge flow, so it requires the two mixing fluids to have the same density (i.e. purge flow must be air for gas turbine applications). In actual engine, the purge flow has an higher density than the main annulus flow because it is colder. Thus, it is necessary to define the density ratio as the cold purge flow density divided by the hot main flow density:

$$DR = \frac{\rho_o}{\rho_{main}} \tag{43}$$

A modified version of the Orifice Model equations is therefore required to account for the density ratio. The latter was proposed by Orsini et al. [33] and is given below (the reader is referred to the relevant article for the derivation of Eq. 44):

$$\frac{\Phi_o}{\Phi_{min,EI}} = \frac{\varepsilon \cdot \sqrt{\rho_e/\rho_o}}{\left[1 + \left(\frac{\Gamma_c}{\sqrt{DR}\cdot\sqrt{\rho_e/\rho_o}}\right)^{-\frac{2}{3}} \cdot (1-\varepsilon)^{\frac{2}{3}}\right]^{\frac{3}{2}}} \tag{44}$$

This new definition also requires an update for the non-dimensional sealing parameter, including the DR:

$$\Phi = DR \cdot \frac{U}{\Omega \cdot b} \tag{45}$$

The same applies to the minimum value of Φ to prevent ingress:

$$\Phi_{min,EI} = \frac{2}{3} \cdot C_{d,e} \cdot \sqrt{DR} \cdot \sqrt{\Delta C_p} \tag{46}$$

In this context, the definition of Φ given in Eq. 45 can be interpreted as a ratio between specific mass flows. Practically speaking, if the test rig is operating at a certain test condition, defined by the annulus mass flow and rotational speed, a specific value of Φ corresponds to a unique value of purge flow rate, apart from its specific density [33].
Eq. 44 includes the contribution of ρ_e/ρ_o which is difficult to calculate. However, as shown in the Figure 4 of Orsini et al. [33], the approximation of $\rho_e/\rho_o = 1$ is acceptable since it has a small effect on the sealing effectiveness on the stator side. This approach

is also used in this report as it simplifies the data analysis and, above all, maintains the specificity of the Orifice Model proposed by Owen by decoupling cause and effect; in addition, the probes for seedgas measurements are installed only on the stator surface of the test rig.

In this work, the Orifice Model was used to find the Γ_c value that best fits the experimental data in terms of (ε, Φ_o). Eq. 40 and Eq. 44 are non linear and were solved using the Mean Square Method, i.e. by finding the optimal Γ_c value that minimizes the quadratic difference between the effectiveness experimental data (ε_{exp}) and the values predicted by the model ($\varepsilon_{mod}(\Gamma_c)$). To calculate the latter, it is first necessary to calculate the minimum non-dimensional sealing parameter. This can be done using Eq. 2.12 of Sangan et al. [7], reported below:

$$\Phi_{min,EI} = K \cdot \sqrt{\frac{\Delta C_p}{2}} \tag{47}$$

K in an empirical constant. Phadke and Owen [34]–[36] examined the influence of EI ingress on the sealing effectiveness for a variety of seals and they correlated their data with $K = 0.6$. The same value is adopted in this thesis. The non-dimensional peak-to-trough pressure difference ΔC_p on the hub is computed from the data acquired during the trials.

Once that the optimal value $\Gamma_{c_{opt}}$ is found, the Orifice Model equation is used to calculate $(\varepsilon_{mod}(\Gamma_{c_{opt}}))$ for the experimental data of Φ_o. The result of applying the model in this way is a plot showing the experimental data and the modelled curve with the optimized value of Γ_c. Since are available only three values of Φ_o for each operating speed of the Test Turbine, two more points were added to the plot to obtain a smoother curve, as listed below:

- $(\varepsilon, \Phi_o) = (0, 0)$
- $(\varepsilon, \Phi_o) = (1, \Phi_{min})$

These two points have not been tested, but it makes sense to add them since theory shows that the sealing effectiveness is zero when there is no purge flow ($\Phi_o = 0$) and that the sealing effectiveness is one when the purge flow is equal to the minimum value to prevent ingress ($\Phi_o = \Phi_{min}$) (mentioned in Sec. 3.3).

3.6 Swirl ratio

As mentioned in Sec. 2.2.6, Facchini et al. [18] used a corrected radial position to account for the fact that the cavity inlet radius is far from the rotational axis, which also occurs in the test rig used in this project. It is defined as:

$$x_{corr} = \frac{r - d}{b - d} \tag{48}$$

Their correlation also considers the turbulent flow parameter, which was first introduced by Owen & Rogers [11]:

$$\lambda_t = C_w \cdot Re_\theta^{-\frac{4}{5}} \tag{49}$$

The resulting correlation is defined below:

$$\beta = \beta^* \cdot \left(1 + 7.55 \cdot \left(\frac{\lambda_t}{x_{corr}^{\frac{13}{5}}}\right) - 13.52 \cdot \left(\frac{\lambda_t}{x_{corr}^{\frac{13}{5}}}\right)^2 + 188.56 \cdot \left(\frac{\lambda_t}{x_{corr}^{\frac{13}{5}}}\right)^3\right)^{-1} \tag{50}$$

β^* is the core swirl ratio when $C_w = 0$, i.e when there is no purge flow. It was quantified as 0.426 by Owen [37].

3.7 Experimental procedure

The stage design pressure ratio of 2.12 was examined by varying the operating speed and the amount of purge mass flow injected into the cavity. The operating speed is defined by the flow coefficient, while the purge rate is defined by the mass flow ratio, respectively expressed as:

$$C_f = \frac{c_{1,x}}{\Omega \cdot b} \tag{51}$$

$$MFR = \frac{\dot{m}_o}{\dot{m}_o + \dot{m_{main}}} \tag{52}$$

In particular, at a given speed, three different mass flow ratios were analyzed. The operating points studied are listed in Table 3.2.

Table 3.2: Investigated operating points

N [rpm]	**C_f** [-]	**MFR**
10540	0.35	0.5%, 1%, 1.5%
14000	0.26	0.5%, 1%, 1.5%

It is very important to remember that the mass flow controllers (MFCs) installed in the laboratory are calibrated for air. For this reason, to perform trials with argon as purge flow, it is necessary to calculate a conversion factor between air and argon, defined as the ratio of argon mass flow to air mass flow, as follows:

$$CF = \frac{\dot{m_{argon}}}{\dot{m_{air}}} \tag{53}$$

The conversion was performed through the Fluidat website (Flow Calculations > Gas Conversion Factor). The model of the mass flow controller (F206-AI), the mass flow rate of air (180 kg/h) and the reference pressure and temperature (1 bar(a), 20°C) should be set. The results of the conversion are illustrated in Figure 3.6: it can be seen that the argon mass flow is higher than air (argon is a heavier gas), so the conversion factor is higher than one.

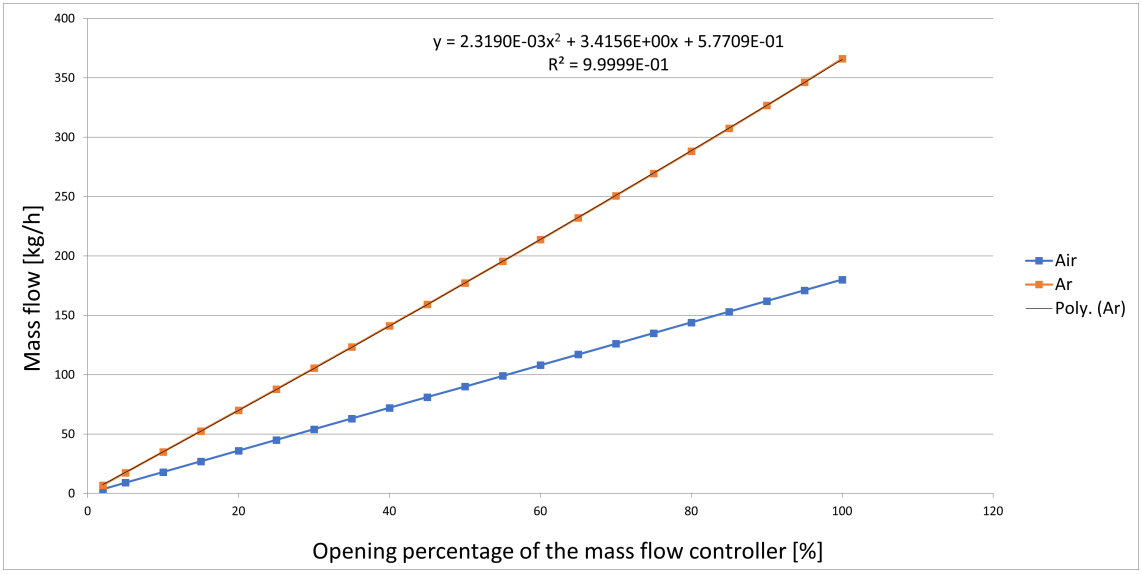

Figure 3.6: Conversion factor air-argon

The main annulus mass flow is known ($\approx 3.5 kg/s$), so it is possible to calculate the purge flow through the Eq. 52. Then, if the purge flow being tested is argon, the air mass flow

with which to feed the MFCs must also be calculated using the conversion factor. The carbon dioxide mass flow used as seedgas is set equal to 1% of the purge flow. However, during the tests there was a problem with the CO_2 mass flow setting program, which did not allow decimal values to be set, so only integer values were set, but this did not affect the results, as a higher amount of CO_2 meant that the gas analyzer reading was higher, but still within the calibrated range of the gas analyzer. The Table 3.3 shows the different mass flows computed for each MFR. Note that the second column refers to the purge mass flow when using air, while the fourth column refers to the purge mass flow when using argon.

Table 3.3: Mass flow rates through the MFCs

MFR	Purge mass flow [kg/h]	CF [-]	Air mass flow [kg/h]	CO2 mass flow [kg/h]
1.5%	193.95	1.974	98.28	3
1%	128.65	1.957	65.73	2
0.5%	64	1.944	32.91	1

As mentioned in Section 3.3, the sealing effectiveness is usually evaluated at different radial locations within the cavity and is defined as follows:

$$\varepsilon = \frac{\gamma_s - \gamma_{inlet}}{\gamma_o - \gamma_{inlet}}$$

Figure 3.7 shows a cross-section of the test turbine, highlighting the cavity, where the numbers refer to the pressure and temperature taps. The radial positions identified for measuring the seedgas concentration to calculate the effectiveness of the seal are listed in the Table 3.4. With reference to Figure 3.7:

- probes number 13, 33, 34, 35, 36 refer to γ_s (they are all on the stator side)
- probe number 9 refers to γ_o
- the probe that refers to γ_{inlet} is not shown as it is located on the settling chamber

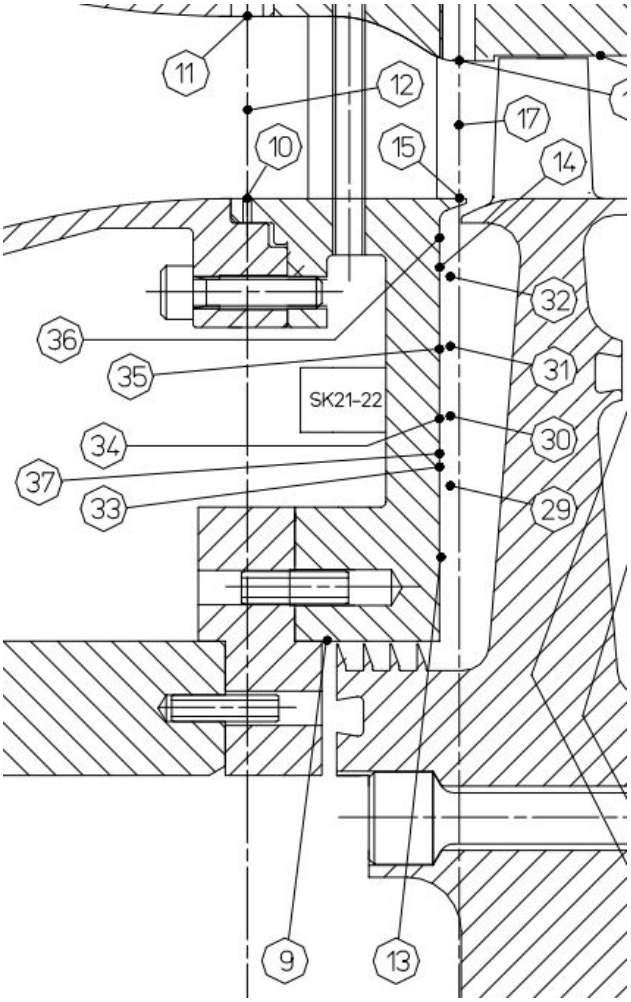

Figure 3.7: KTH Test Turbine cavity (granted by Siemens Energy)

Table 3.4: Measurement locations within the cavity

Pos no.	X-pos	R-pos	FI-pos
9	1917.2	95	95
13	1939.2	105	210
33	1939.2	127.5	210
34	1939.2	136.5	210
35	1939.2	149.5	210
36	1939.2	170.2	209.284

4 Results

In this section the results of the degree project concerning the sealing effectiveness, the efficiency and the Orifice Model are presented. During the trials, only steady measurements were taken, which means that the Traverse equipment (mentioned in Sec. 3.1.3) was not used. The data acquired were computed both in an online Excel programme provided by Siemens and through a MATLAB code written and updated by previous researchers who worked on the Test Turbine (however, density ratio studies have never been done on the test rig, so the code required some modifications, especially regarding gas constants).

The reported results are divided between design and off-design conditions. The C_f was calculated from the ratio of the axial to the rotational Reynolds number, both defined using the main annulus density; its value on-desing (i.e 10540 rpm) is $C_f = 0.35$, while off-desing (i.e. 14000 rpm) it is $C_f = 0.26$. For each of the latter operating speeds, three different purge flow rates (i.e. MFR) were tested, using both air (DR=1) and argon (DR=1.38) as purge gas. The DR was calculated by considering the same reference point in terms of pressure and temperature for purge and main annulus flow. However, the influence of reference pressure and temperature can be neglected as the density of an ideal gas is directly proportional to pressure and inversely proportional to temperature. The ideal gas assumption is justified by the fact that pressures are not too high and temperatures are not too low.

Below are the values of the non-dimensional sealing parameter Φ_o by varying the test rig speed and the MFR, as they are useful for understanding the following figures.

Table 4.1: Values of Φ_o varying C_f and MFR

C_f [-]	0.35	0.26
MFR		
0.5%	0.025	0.019
1%	0.050	0.037
1.5%	0.075	0.056

4.1 Sealing effectiveness

The sealing effectiveness trends within the cavity are shown in the Figures 4.1, 4.2. Please note that the correct hub radius is b=0.1775 m, but only to compute the sealing effectiveness, b=0.173 m was used to compare the results with those obtained by the last research engineer working on the Test Turbine (Arijit Sinha Roy) who used this value (see Section 4.1.1).

For both purge gases, an increase in ε can be observed as Φ_o increases, thus increasing the amount of purge flow. Also, regardless of the gas, the sealing level should increase as the radius inside the cavity decreases; indeed, at higher radius there is the mixing with the main annulus flow entering the cavity, so the effectiveness of the seal is lower. This trend is not verified for all the testing conditions, in particular for both gases at $C_f = 0.35$ and $\Phi_o = 0.025$, for both gases at $C_f = 0.26$ and $\Phi_o = 0.037$, and for argon at $C_f = 0.26$ and $\Phi_o = 0.056$. Furthermore, what has just been said implies that the lowest effectiveness value occurs at the highest radius, just below the rim seal.

For a given purge gas and a constant MFR, as C_f increases, and therefore the non-dimensional pressure difference ΔC_p, which is the driving force for EI ingress, the effectiveness of the seal to prevent this ingress decreases. This is because the purge gas must overcome a larger pressure difference to prevent the annulus fluid from entering the wheel space, making it less effective in sealing the cavity. To preserve effectiveness, the purge gas flow rate must be increased to counterbalance the stronger ingress driving force, or the seal design must be improved to reduce ingress.

Before analyzing the influence of the DR at a specific value of Φ_o, it is important to remember that comparing Φ_o between different gases assumes the injection of the same amount of purge flow into the cavity without taking into account the different densities of the purge gases (see Eq. 45).

If the same quantity of purge mass flow is injected into the cavity, a similar ε trend occurs for the two gases but the use of an heavier gas results in lower sealing effectiveness and therefore lower protection. Lower effectiveness could be explained by the different velocities assumed by the purge flow according to the density difference. However, this is not verified everywhere within the cavity under off-design conditions for $\Phi_o = 0.037$ and $\Phi_o = 0.056$; the reason for this is analyzed in Section 4.4.

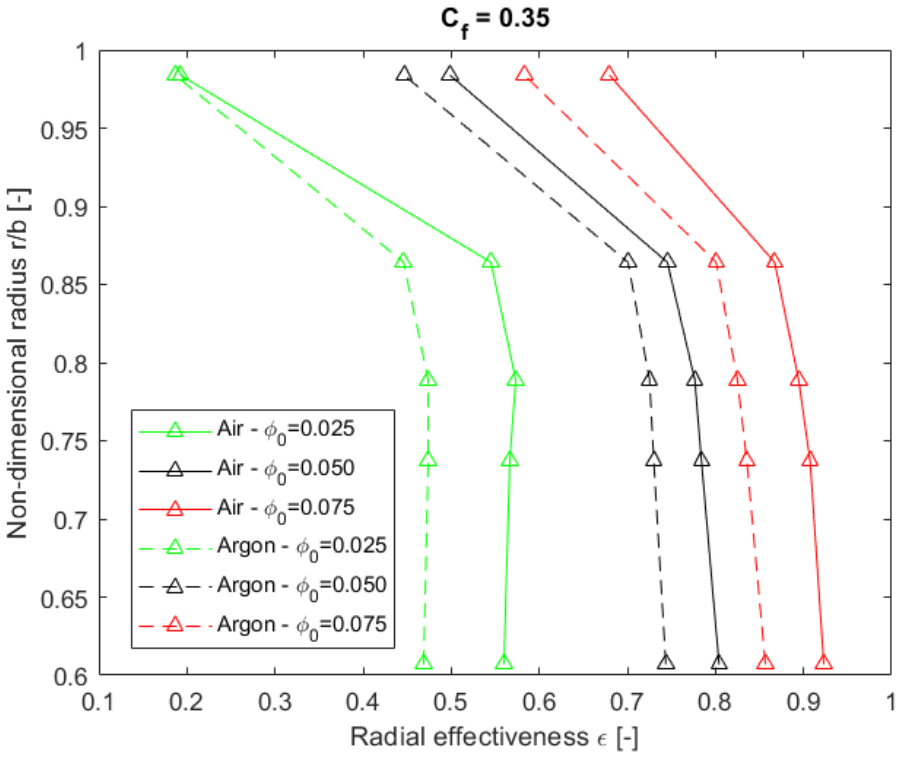

Figure 4.1: Sealing effectiveness, on-design

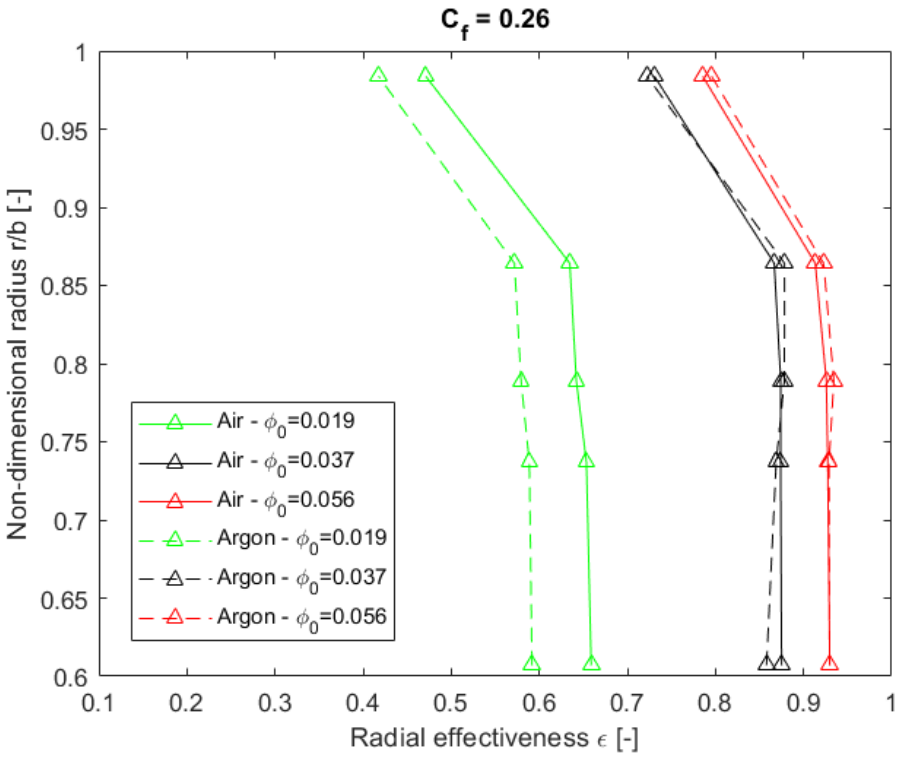

Figure 4.2: Sealing effectiveness, off-design

4.1.1 Sealing effectiveness comparison on-design

It is possible to compare the sealing effectiveness values with those previously obtained in the laboratory, but only with air as purge flow and at design point ($C_f = 0.35$) because argon has never been tested in the laboratory. This is shown in Figure 4.3. Note that the Blisks are different but the radial measurement locations within the cavity are the same. Also, only black and red trends can be compared since the blue trend refers to a MFR not tested in the thesis project. It can be seen that the trends largely match, except for the highest radius. The reason for this is probably that when flowing air within the cavity, there is no risk of running out of air as it is taken from the atmosphere, so it had previously been possible to make measurements of probes placed circumferentially at the highest radius and then average them. On the other hand, this was not possible in this work because argon, which is an expensive gas, was also tested. However, the trials with air could have been carried out by taking several circumferential probes at the same radius, but this was not done because the purpose of the thesis is to compare the results between air and argon as purge flow.

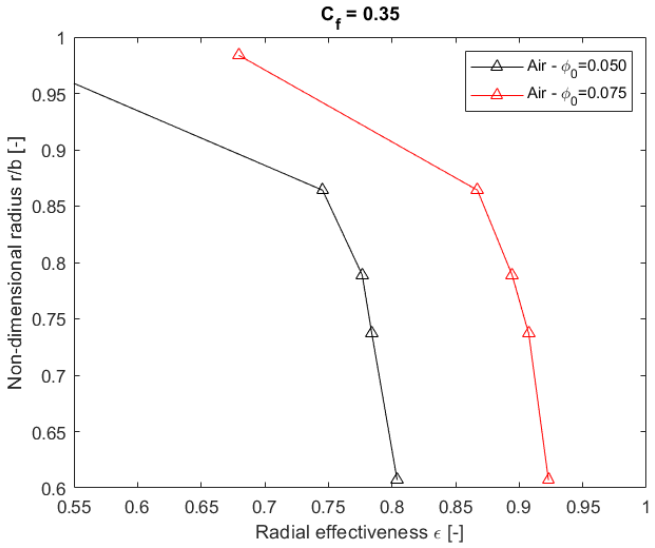

Blisk 6

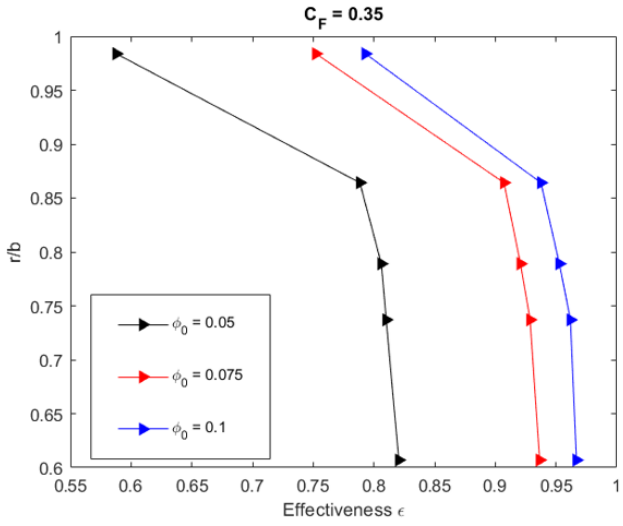

Blisk 5. Granted by A. S. Roy

Figure 4.3: Sealing effectiveness comparison with air as purge flow (on-design)

4.2 Efficiency

The results obtained for the total-to-total and total-to-static efficiency, both on-design and off-design, are reported in Figures 4.4, 4.5, 4.6, 4.7. The efficiency values are within the uncertainty bar (the reader is referred to Chapter 6 of Dahlqvist [3] for the uncertainty estimation). Also, as can be expected, the efficiency decreases as the MFR increases because more cooling flow is injected into the cavity.

For the same purge mass flow rate (i.e. same Φ_o), the use of an heavier purge gas appears to result in lower values for both efficiencies. This trend is verified for all the testing conditions, except for the highest value of Φ_o at the off-design point. However, for $\Phi_o = 0.056$, the total-to-total efficiency of argon is only 0.07% higher than that of air, while the total-to-static efficiency of argon is only 0.08% higher than that of air. This can be attributed to the uncertainty of the measuring instruments.

By varying the Φ_o, almost the same gap exists between the total-to-total and total-to-static efficiency of air and argon under design conditions, while under off-design conditions this is true only for the highest value of Φ_o.

4.2.1 Total-to-total efficiency

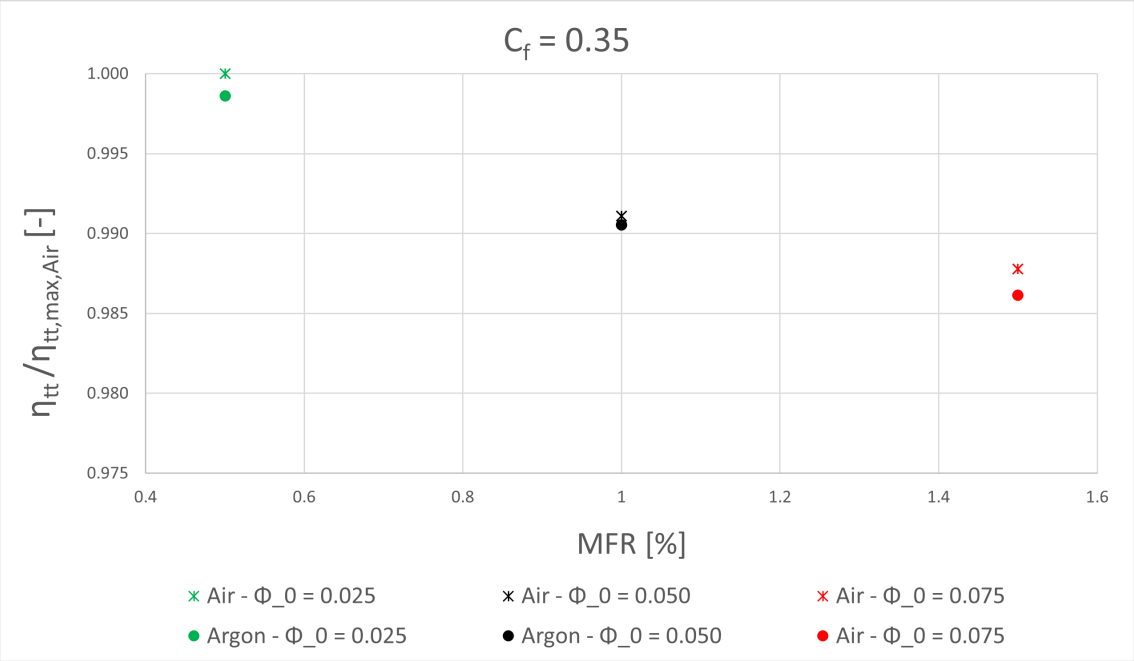

Figure 4.4: Total-to-total efficiency, on-design

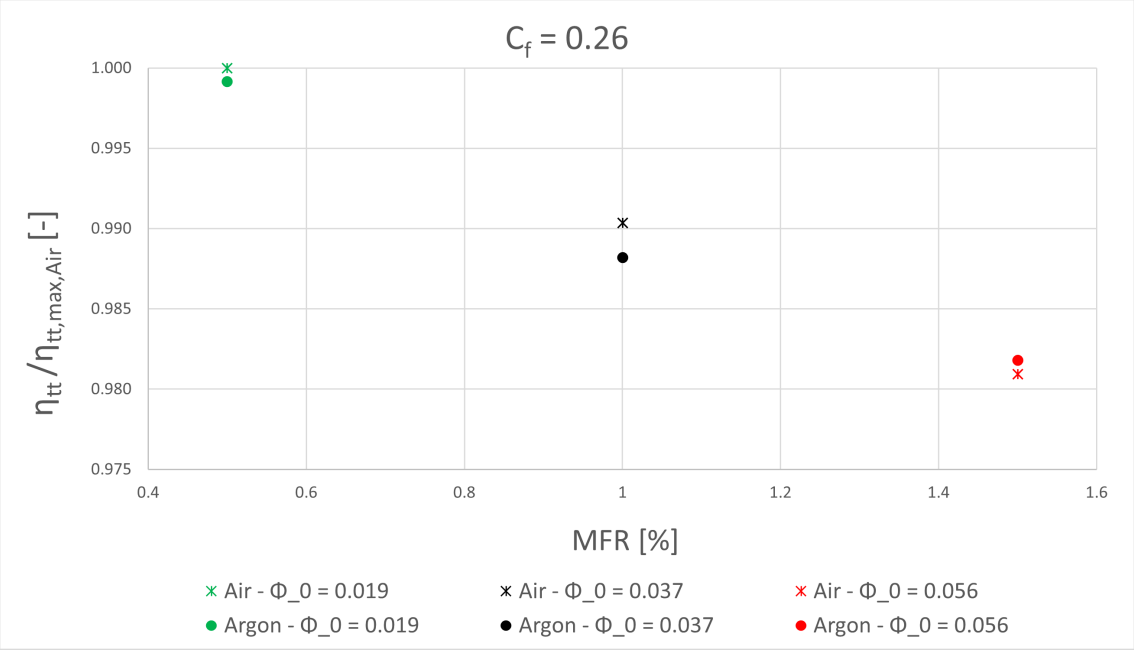

Figure 4.5: Total-to-total efficiency, off-design

4.2.2 Total-to-static efficiency

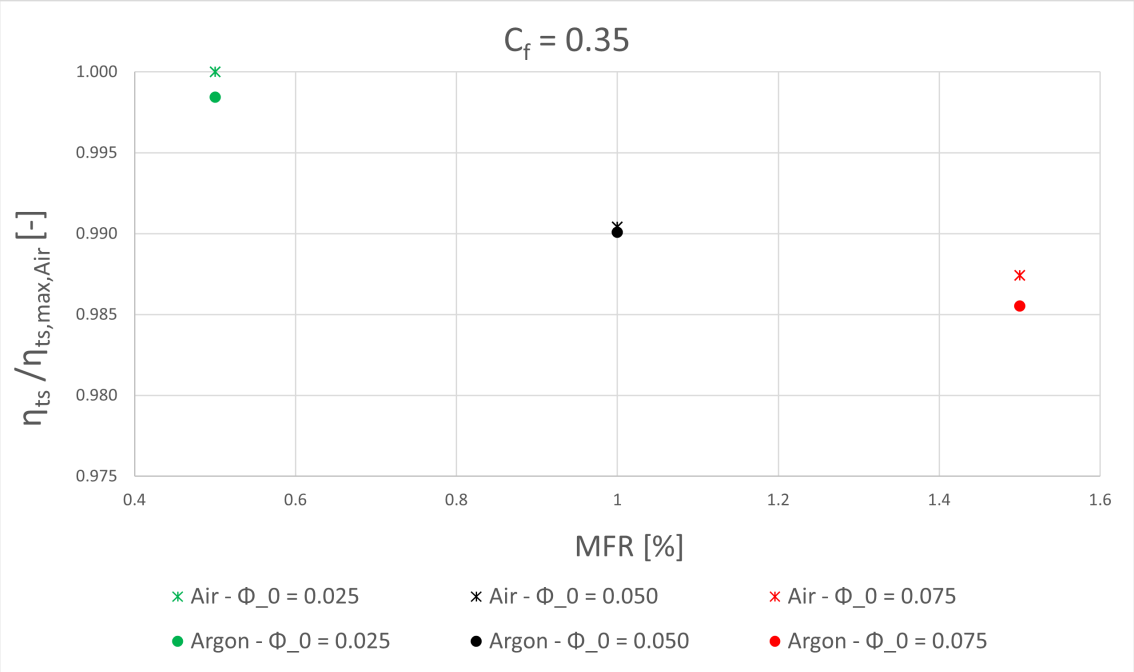

Figure 4.6: Total-to-static efficiency, on-design

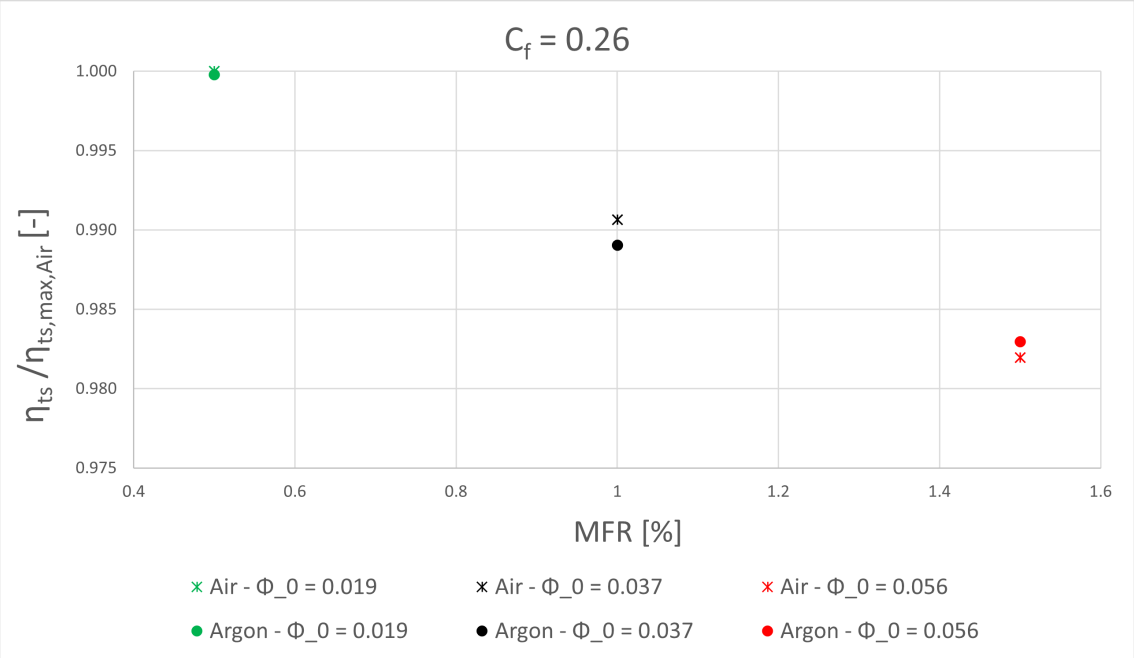

Figure 4.7: Total-to-static efficiency, off-design

4.3 Orifice Model

As mentioned in Sec. 3.5, the OM was used to find the optimal Γ_c value that fits the experimental data in terms of (ε, Φ_o). As the effectiveness ε varies with radius, a radius must be chosen in which to apply the OM equation. Since the mixing between the main annulus flow entering the cavity and the purge flow occurs below the rim seal, the radial location chosen is the highest measuring probe within the cavity (pos. no. 36 in Figure 3.7). The results are shown in the figures below.

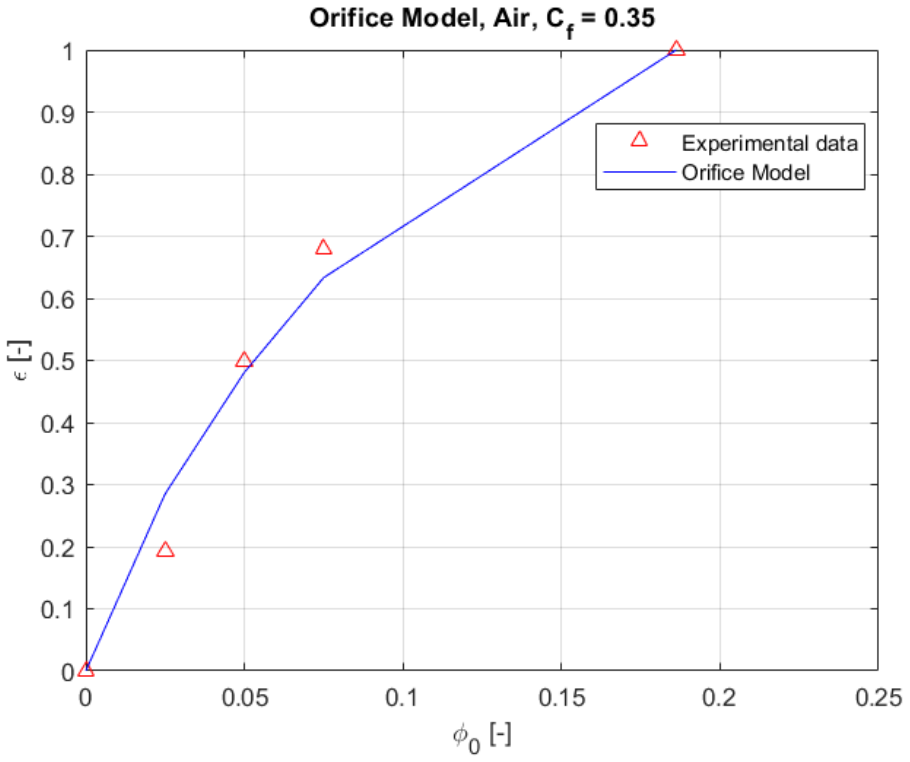

Figure 4.8: Optimal Γ_c with air as purge flow, on-design

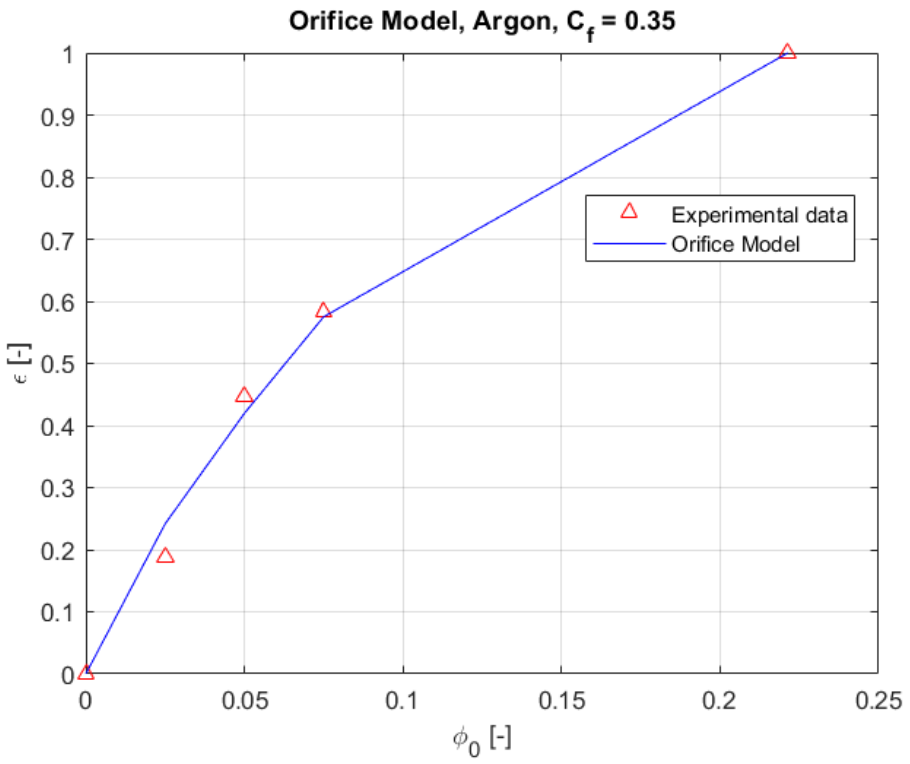

Figure 4.9: Optimal Γ_c with argon as purge flow, on-design

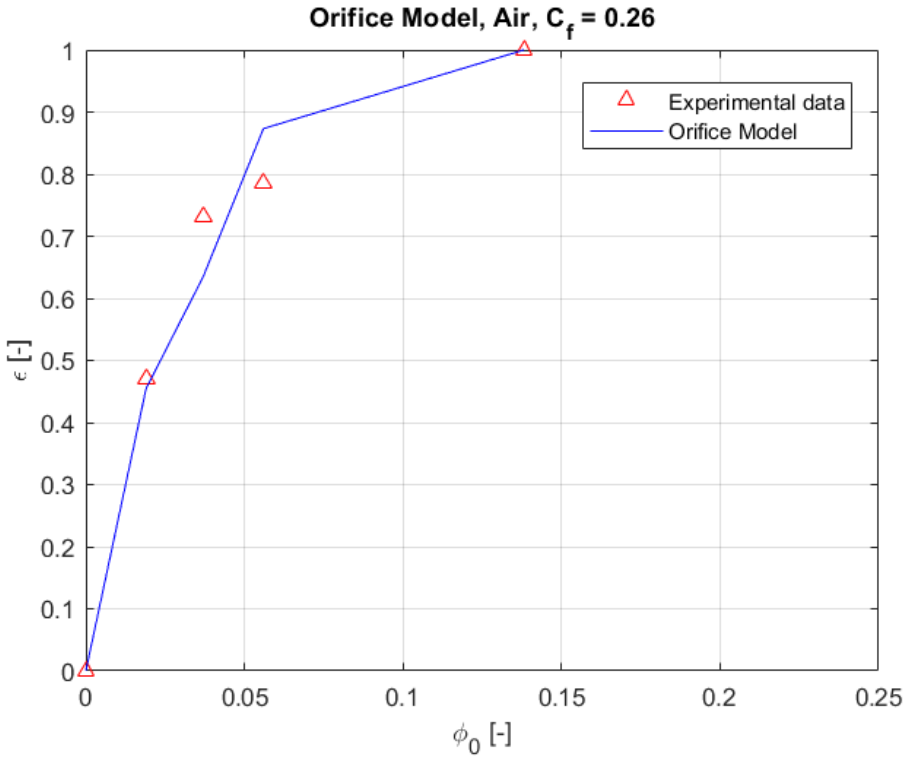

Figure 4.10: Optimal Γ_c with air as purge flow, off-design

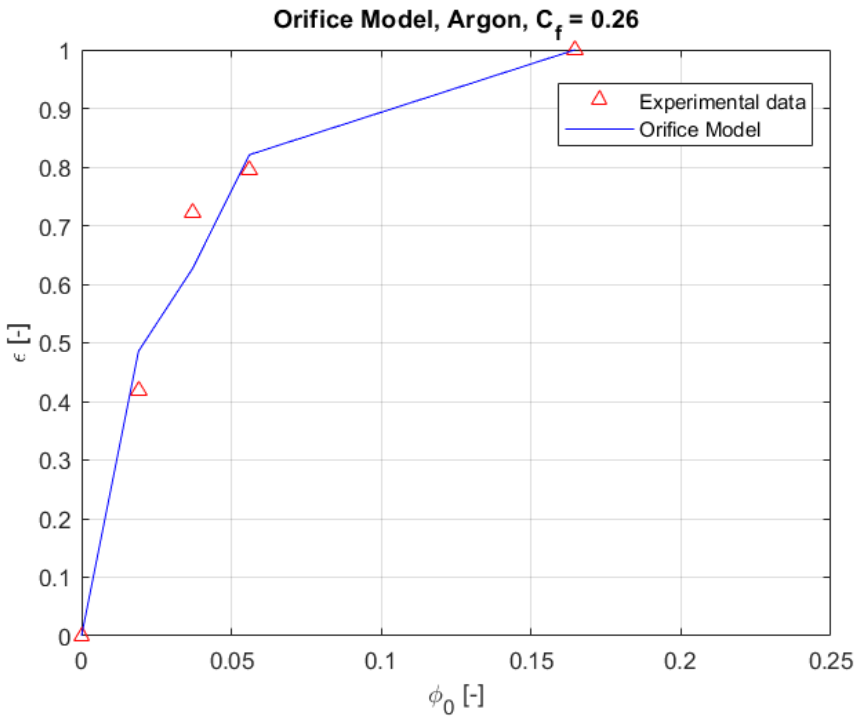

Figure 4.11: Optimal Γ_c with argon as purge flow, off-design

4.3.1 Comparison of the optimal fitting parameters

The Table 4.2 provides a summary of the results from the OM data interpolation used to derive the trends shown in Figures 4.8, 4.9, 4.10, 4.11. The results refer to the two operating speeds tested, both for DR=1 and DR=1.38, to analyze the effect of the DR. First of all, it is important to note that ΔC_p, which is the driving force for EI ingress, is independent from the purge density and its value depends only on the operating point. In particular, ΔC_p increases as C_f increases (i.e. as the test rig speed decreases). The Φ_{min} differs between the two gases, and when using a lower density fluid as purge flow, a smaller mass flow rate is required to prevent ingress. The ratio $\frac{\Phi_{min,Argon}}{\Phi_{min,Air}}$ is almost constant by varying the rotor angular velocity (i.e. C_f) and seems to be closely approximated by the square root of the DR, confirming the results in literature [33]. Therefore, for a given C_f (and so for a given ΔC_p), it can be deduced from Eq. 46 that the value of of $C_{d,e}$ is not affected by the density of the gas used as purge flow.

If the ratio between $\Gamma_{c,Argon}$ and $\Gamma_{c,Air}$ had been very close to 1 for each operating speed, then the OM curve would have had the same shape regardless of the purge flow density and, since the DR does not influence the $C_{d,e}$, also the $C_{d,i}$ would not have been affected by the density of the gas injected into the cavity. This also would have confirmed the literature results but does not occur in this work because the ratio is not too close to 1.

Table 4.2: Comparison of the optimal fitting parameters Φ_{min} and Γ_c

Orifice Model fitting	C_f = 0.35		C_f = 0.26	
	Air	**Argon**	**Air**	**Argon**
$\sqrt{\mathbf{DR}}$	1	1.1747	1	1.1747
$\boldsymbol{\Delta C_p}$	0.1925	0.1972	0.1060	0.1092
$\frac{\boldsymbol{\Phi_{min,Argon}}}{\boldsymbol{\Phi_{min,Air}}}$	1.1889		1.1921	
$\frac{\boldsymbol{\Gamma_{c,Argon}}}{\boldsymbol{\Gamma_{c,Air}}}$	1.1605		0.8550	

4.4 Swirl ratio

According to Eq. 50, the swirl ratio β depends on the radial position within the cavity in which calculate x_{corr} (Eq. 48). Since the mixing between the main annulus flow entering the cavity and the purge flow occurs below the rim seal, the radial location chosen is the hub radius. Therefore, β is the ratio between the tangential velocity of the flow exiting the seal and the rotor tangential velocity at the hub radius. From Table 4.3, it can be seen that increasing the MFR, the swirl ratio β decreases for both air and argon at each operating speed. A lower value of β indicates that the purge flow is directed more in the axial direction, which increases the seal cross-sectional area available for exit, resulting in a lower exit velocity through the seal.

This parameter is also useful to check whether any compressibility effect occurs within the cavity. In this regard, the swirl velocity and the corresponding Mach number were calculated, at the same radial location of β. The reason for checking if the incompressibility hypothesis is still valid is that at the maximum operating speed the trend shown in Figure 4.2 for $\Phi_o = 0.037$ and $\Phi_o = 0.056$ does not follow the theory. In particular, it is not satisfied everywhere within the cavity that the sealing effectiveness is lower when an heavier purge flow is used. Considering $M \approx 0.3$ as the threshold of incompressibility, it can be deduced from Table 4.3 that no major compressibility effects occur in the cavity.

Table 4.3: Swirl ratio and swirl Mach number within the cavity

	$C_f = 0.35$			$C_f = 0.26$		
	MFR=0.5%	**MFR=1%**	**MFR=1.5%**	**MFR=0.5%**	**MFR=1%**	**MFR=1.5%**
β_{Air}	0.3088	0.2314	0.1697	0.3261	0.2594	0.2043
β_{Argon}	0.3326	0.2687	0.2154	0.3468	0.2904	0.2446
$\mathbf{M}_{Air}$	0.1664	0.1248	0.0926	0.2297	0.1839	0.1456
$\mathbf{M}_{Argon}$	0.1916	0.1551	0.1246	0.2598	0.2174	0.1842

5 Conclusions

Increasing the turbine inlet temperature to improve gas turbine performance requires, among other cooling techniques, the use of cavity purge flow to keep the wheel space between stator and rotor at safe temperatures and prevent damage to turbine components. Studies on this topic began around 1950 with the growing interest in gas turbines, especially in the aviation sector, but more detailed numerical and experimental activities have been carried out only since the 1990s. CFD codes have been developed but simulations are expensive and time-consuming, so a good option is to use the models and correlations developed by some researchers in the past few years. The latter have required the acquisition of experimental data by performing several tests on experimental rigs, which are designed to operate similarly to engine operating conditions. These data are also useful for the validation of CFD codes.

In real engines, both for aviation and power generation, the purge flow is bled from the compressor, so it is the same gas flowing into the main annulus, but it is colder and therefore there is a difference in density between these two mixing fluids. However, the majority of experimental test rigs work under cold flow conditions so it is not possible to reproduce real engine conditions in which, usually, the main flow after the combustion chamber is at around 1400 °C, while the cavity flow is bled from the compressor at around 400 °C. This means that the effect of the density difference is neglected. To overcome this problem, the test rig used in this thesis project allowed for testing different density ratios by injecting air (DR=1) or argon (DR=1.38) into the wheel space. The key findings obtained throughout the project are reported below.

If the same quantity of purge mass flow is injected into the cavity, the DR does not affect the trend of the $r/b - \varepsilon$ curve, but the use of an heavier gas leads to lower sealing effectiveness, and therefore lower protection. This could be explained by the different velocities assumed by the purge flow according with the density difference. The matching with previous results using air as purge flow and at the design point strengthens the effectiveness results obtained.

Efficiency values are within the uncertainty bar. For the same purge mass flow rate, the use of an heavier gas seems to lead to lower efficiency values. Also, the efficiency decreases as the MFR increases because more cooling flow is injected into the cavity.

Then, the effectiveness results were used to calibrate the original Orifice Model and a

modified version that take into account the DR. This allowed to find the optimal Γ_c value that fits the experimental data in terms of (ε, Φ_o) and to analyze the effect of the DR on the performance of the seal. Also, it was found that ΔC_p, earlier believed as one of the drivers for EI ingress, is independent from the purge density and its value depends only on the operating point, increasing as C_f increases. The ratio between $\Phi_{min,Argon}$ and $\Phi_{min,Air}$ is almost constant by varying the rotor angular velocity and it is well approximated by the square root of the DR, confirming the results in literature.
In the end, the swirl ratio and the resulting swirl Mach number were calculated to check whether any compressibility effect occurs within the cavity. It was observed that increasing the MFR, the swirl ratio decreases for both purge gases at each operating speed, meaning that the purge flow is directed more in the axial direction. The swirl Mach number values suggested that no major compressibility effects occur into the cavity.
The conclusions of this project offer a valid tool for predicting the minimum purge mass flow required to seal the cavity (i.e. Φ_{min}) and the appropriate amount of purge to achieve a good trade-off between efficiency and safe operating temperatures. Also, in cases where experimental data are available only at DR close to one, for estimating cavity behavior at engine-like density conditions, i.e. to extrapolate results obtained in a test rig operating at low pressures and low temperatures to the engine operating conditions.

5.1 Future Works

To obtain more reliable fit parameters using the Orifice Model, it will probably be necessary to test a much larger number of mass flow ratios. If the ratio between $\Gamma_{c,Argon}$ and $\Gamma_{c,Air}$ is close to 1 for each operating speed, it means that the Orifice Model curve has the same shape regardless of the purge flow density, confirming the results in literature. In this project it did not occur, but testing a much larger number of mass flow ratios may alter the conclusion. Also, it is worth to validate the modified version of the Orifice Model with much more test campaigns, since it was recently proposed.
The test rig used allow also for unsteady measurement through the traverse instrumentation. During this project, only steady measurements were made due to some problems that occurred in the experiments and that took time to fix, as well as completely depleting the argon supply available in the laboratory. It is therefore a good option to perform traverse measurements to quantify the mixing process in the axial direction.
It is important to note that the pressure and temperature taps are distributed only along the

stator side of the wheel space, thus allowing to obtain results only for this side. It might be useful to install taps on the rotor surface as well and compare the results with those obtained on the stator and others available in the literature.

To look for an answer to the unusual trend in Figure 4.2 for $\Phi_o = 0.037$ and $\Phi_o = 0.056$, the tangential velocity of the flow exiting the seal was calculated. However, the proper velocity component to study should be the radial one, which is likely to be quite different at the different operating points. In fact, this makes sense considering what happens in the disc pumping effect: the cavity flow coming from the bottom is entrained in the rotor boundary layer and then follows the rotor side radially towards the rim seal, where it interacts with the main annulus flow.

The models and correlations are useful to understand the causes of losses formation, such as mixing between the purge flow and the main annulus flow. However, for a better understanding of the experimental results, it is worth to perform CFD simulations under the same operating conditions as the experimental tests to allow comparison of results, which should be almost the same to validate the model, otherwise it should be corrected. Indeed, experiments may be affected by the uncertainty of the instruments and by human errors that could occur in the machine manufacturing steps or in the setup phase. On the opposite, the model is not affected by these errors. For example, due to obvious manufacturing errors, it might happen that some surfaces have a roughness a bit different from the designed one, so the flow in these areas will be different from the one studied in the model. Nevertheless, CFD simulations have not been carried out during the project due to lack of time and of the cavity model for the Blisk analyzed, but are planned for the future. In detail, the cavity will be modeled together with the rotating domain, then together with the rotor disk, while the stator disk is modeled separately from the latter.

References

[1] Winterbone, D. E. and Turan, A., *Advanced thermodynamics for engineers*, 2nd edition. Boston Butterworth-Heinemann, 2015, ISBN: 978-0-444-63373-6.

[2] Baskharone,
E. A. and Hill, D. L., "Introduction to gas turbine engines," in *Principles of Turbomachinery in Air-Breathing Engines*, Cambridge University Press, Oct. 19, 2023, pp. 1–7, ISBN: 978-1-108-64893-6. DOI: 10.1017/9781108648936. [Online]. Available: https://www.cambridge.org/highereducation/books/principles-of-turbomachinery-in-air-breathing-engines/698A18888776F4A0B05BB4420170453B/introduction-to-gas-turbine-engines/E7D55549F10F43410DCD64BAF9E7216D.

[3] Dahlqvist, J., "Cavity purge flows in high pressure turbines," ISBN: 978-91-7729-626-3 (ISBN) Number Of Volumes: Report 17/07 Publication Title: TRITA-KRV Report 17/07, Doctoral thesis, comprehensive summary, KTH Royal Institute of Technology, Stockholm, 2017, 62 pp. [Online]. Available: http://urn.kb.se/resolve?urn=urn:nbn:se:kth:diva-218468.

[4] Denton, J. D., "The 1993 IGTI scholar lecture: Loss mechanisms in turbomachines," *Journal of Turbomachinery*, vol. 115, no. 4, pp. 621–656, Oct. 1, 1993, ISSN: 0889-504X. DOI: 10.1115/1.2929299. [Online]. Available: https://doi.org/10.1115/1.2929299 (visited on 10/11/2024).

[5] Agromayor, R. and Nord, L. O., "Preliminary design and optimization of axial turbines accounting for diffuser performance," *International Journal of Turbomachinery, Propulsion and Power*, vol. 4, no. 3, p. 32, Sep. 2019, Number: 3 Publisher: Multidisciplinary Digital Publishing Institute, ISSN: 2504-186X. DOI: 10.3390/ijtpp4030032. [Online]. Available: https://www.mdpi.com/2504-186X/4/3/32.

[6] Lewis, R. I., *Turbomachinery performance analysis*. Butterworth-Heinemann, 1996, ISBN: 978-0-340-63191-1.

[7] Sangan, C. M., Pountney, O. J., Zhou, K., Wilson, M., Michael Owen, J., and Lock, G. D., "Experimental measurements of ingestion through turbine rim seals—part i: Externally induced ingress," *Journal of Turbomachinery*, vol. 135, no. 2, p. 021 012,

Mar. 1, 2013, ISSN: 0889-504X, 1528-8900. DOI: 10.1115/1.4006609. [Online]. Available: https://asmedigitalcollection.asme.org/turbomachinery/article/doi/10.1115/1.4006609/378497/Experimental-Measurements-of-Ingestion-Through.

[8] Royce, R., *The Jet Engine*. John Wiley & Sons, Jul. 20, 2015, 291 pp., Google-Books-ID: QUQxBwAAQBAJ, ISBN: 978-1-119-06599-9.

[9] "Boundary layers and free shear layers," in *Internal Flow: Concepts and Applications*, ser. Cambridge Engine Technology Series, E. M. Greitzer, C. S. Tan, and M. B. Graf, Eds., Cambridge: Cambridge University Press, 2004, pp. 166–216, ISBN: 978-0-521-03672-6. DOI: 10.1017/CBO9780511616709.006. [Online]. Available: https://www.cambridge.org/core/product/40675025D8A72A907D25DEB829DA83CE.

[10] Scobie, J. A., Sangan, C. M., Michael Owen, J., and Lock, G. D., "Review of ingress in gas turbines," *Journal of Engineering for Gas Turbines and Power*, vol. 138, no. 12, p. 120 801, Dec. 1, 2016, ISSN: 0742-4795, 1528-8919. DOI: 10.1115/1.4033938. [Online]. Available: https://asmedigitalcollection.asme.org/gasturbinespower/article/doi/10.1115/1.4033938/474080/Review-of-Ingress-in-Gas-Turbines.

[11] Chapman, C. J., "Flow and heat transfer in rotating-disc systems. volume 1. rotor—stator systems. by j. m. OWEN and r. h. ROGERS. wiley, 1989.," *Journal of Fluid Mechanics*, vol. 241, pp. 724–725, 1992, Edition: 2006/04/26 Publisher: Cambridge University Press, ISSN: 0022-1120. DOI: 10.1017/S0022112092222217. [Online]. Available: https://www.cambridge.org/core/product/8FF6DBE96F3A0FD29A1B1DE2CEBDCDD0.

[12] Childs, P. R. N., *Rotating flow*. Amsterdam Boston: Elsevier, 2011, ISBN: 978-0-12-382098-3.

[13] Daily, J. W. and Nece, R. E., "Chamber dimension effects on induced flow and frictional resistance of enclosed rotating disks," *Journal of Basic Engineering*, vol. 82, no. 1, pp. 217–230, Mar. 1, 1960, ISSN: 0021-9223. DOI: 10.1115/1.3662532. [Online]. Available: https://asmedigitalcollection.asme.org/fluidsengineering/article/82/1/217/397626/Chamber-Dimension-Effects-on-Induced-Flow-and.

[14] Owen, J. M., "Prediction of ingestion through turbine rim seals—part 2: Externally induced and combined ingress," *Journal of Turbomachinery*, vol. 133, no. 3, p. 031 006, Jul. 1, 2011, ISSN: 0889-504X, 1528-8900. DOI: 10.1115/1.4001178. [Online]. Available: https://asmedigitalcollection.asme.org/turbomachinery/article/doi/10.1115/1.4001178/476405/Prediction-of-Ingestion-Through-Turbine-Rim.

[15] Bru Revert, A., Beard, P. F., and Chew, J. W., "Flow and ingestion in a turbine disc cavity under rotationally-dominated conditions," *International Journal of Turbomachinery, Propulsion and Power*, vol. 6, no. 3, 2021, ISSN: 2504-186X. DOI: 10.3390/ijtpp6030029.

[16] Mear, L. I., Owen, J. M., and Lock, G. D., "Theoretical model to determine effect of ingress on turbine discs," in *Volume 5C: Heat Transfer*, Montreal, Quebec, Canada: American Society of Mechanical Engineers, Jun. 15, 2015, V05CT15A005, ISBN: 978-0-7918-5673-4. DOI: 10.1115/GT2015-42326. [Online]. Available: https://doi.org/10.1115/GT2015-42326.

[17] Dahlqvist, J. and Fridh, J., "Purge flow impact on turbine stage and seal performance at varying cavity purge rates and operating speed," *International Journal of Turbomachinery, Propulsion and Power*, 2017. [Online]. Available: http://urn.kb.se/resolve?urn=urn:nbn:se:kth:diva-218465.

[18] Facchini, B., Massini, D., Picchi, A., Micio, M., Bavassano, F., and Mantero, M., "Experimental investigation of swirl and flow structure inside a rotor-stator cavity," in *Volume 5C: Heat Transfer*, Montreal, Quebec, Canada: American Society of Mechanical Engineers, Jun. 15, 2015, V05CT15A013, ISBN: 978-0-7918-5673-4. DOI: 10.1115/GT2015-42852. [Online]. Available: https://asmedigitalcollection.asme.org/GT/proceedings/GT2015/56734/Montreal,%20Quebec,%20Canada/237378.

[19] Salvadori, S., Insinna, M., and Martelli, F., "Unsteady flows and component interaction in turbomachinery," *International Journal of Turbomachinery, Propulsion and Power*, vol. 9, no. 2, p. 15, Apr. 5, 2024, ISSN: 2504-186X. DOI: 10.3390/ijtpp9020015. [Online]. Available: https://www.mdpi.com/2504-186X/9/2/15.

[20] Świrydczuk, J., "Development of vortex structures in a turbine stage rotor passage," *TASK Quarterly. Scientific Bulletin of Academic Computer Centre in Gdansk*, vol. 12, pp. 147–158, 2008.

[21] Burd, S. W., Satterness, C. J., and Simon, T. W., "Effects of slot bleed injection over a contoured endwall on nozzle guide vane cooling performance: Part i — flow field measurements," in *GT2000*, V003T01A007, Volume 3: Heat Transfer; Electric Power; Industrial and Cogeneration, May 8, 2000. DOI: 10.1115/2000-GT-0199. [Online]. Available: https://doi.org/10.1115/2000-GT-0199.

[22] Burd, S. W., Satterness, C. J., and Simon, T. W., "Effects of slot bleed injection over a contoured EndWall on nozzle guide vane cooling performance: Part II — thermal measurements," in *GT2000*, V003T01A008, Volume 3: Heat Transfer; Electric Power; Industrial and Cogeneration, May 8, 2000. DOI: 10.1115/2000-GT-0200. [Online]. Available: https://doi.org/10.1115/2000-GT-0200.

[23] Rehder, H.-J. and Dannhauer, A., "Experimental investigation of turbine leakage flows on the three-dimensional flow field and endwall heat transfer," *Journal of Turbomachinery*, vol. 129, no. 3, pp. 608–618, Jul. 20, 2006, ISSN: 0889-504X. DOI: 10.1115/1.2720484. [Online]. Available: https://doi.org/10.1115/1.2720484.

[24] Ong, J., Miller, R. J., and Uchida, S., "The effect of coolant injection on the endwall flow of a high pressure turbine," *Journal of Turbomachinery*, vol. 134, no. 51003, May 7, 2012, ISSN: 0889-504X. DOI: 10.1115/1.4003838. [Online]. Available: https://doi.org/10.1115/1.4003838.

[25] Song, L., Zhu, P., Li, J., and Feng, Z., "Effect of purge flow on endwall flow and heat transfer characteristics of a gas turbine blade," *Applied Thermal Engineering*, vol. 110, pp. 504–520, Jan. 5, 2017, ISSN: 1359-4311. DOI: 10.1016/j.applthermaleng.2016.08.172. [Online]. Available: https://www.sciencedirect.com/science/article/pii/S1359431116315319.

[26] "Cavity purge flows inside axial turbines," KTH. (), [Online]. Available: https://www.energy.kth.se/heat-and-power-technology/current-projects/cavity-purge-flows-inside-axial-turbines-1.928715.

[27] Södergård, B., Henriksson, K., Kjellström, B., and Söderberg, O., "Turbine testing facility at the department of thermal engineering," KTH - Royal Institute of Technology, Stockholm, Sweden, 1989, TRITA-KRV-1989-03 ISSN: 1100-7990 SE-10044.

[28] Schmidt, G. and Mikaillian, N., "KTH test turbine: Intro & blade aero design," May 2021, Technical project report, Siemens Energy AB.

[29] Fridh, J., "Test turbine commissioning report," ECM-KTH-20240104, 2024.

[30] Salas, M. G. and Roy, A., "Mechanical integrity analysis report," Aug. 2021, Technical project report, Division of Heat and Power Technology, KTH - Royal Institute of Technology.

[31] Dahlqvist, J., Fridh, J., and Fransson, T. H., "TEST TURBINE INSTRUMENTATION FOR CAVITY PURGE INVESTIGATIONS," in *The XXII Symposium on Measuring Techniques in Turbomachinery, Lyon, 4-5 September 2014*, Lyon, Sep. 4, 2014. [Online]. Available: http://urn.kb.se/resolve?urn=urn:nbn:se:kth:diva-181479.

[32] Owen, J. M., "Prediction of ingestion through turbine rim seals—part 1: Rotationally induced ingress," *Journal of Turbomachinery*, vol. 133, no. 3, p. 031 005, Jul. 1, 2011, ISSN: 0889-504X, 1528-8900. DOI: 10.1115/1.4001177. [Online]. Available: https://asmedigitalcollection.asme.org/turbomachinery/article/doi/10.1115/1.4001177/476367/Prediction-of-Ingestion-Through-Turbine-Rim.

[33] Orsini, L., Picchi, A., Facchini, B., Bonini, A., and Innocenti, L., "Impact of the purge flow density ratio on the rim sealing effectiveness in hot gas ingestion measurements," in *Volume 7B: Heat Transfer — General Interest/Additive Manufacturing Impacts on Heat Transfer; Internal Air Systems; Internal Cooling*, Boston, Massachusetts, USA: American Society of Mechanical Engineers, Jun. 26, 2023, V07BT14A023, ISBN: 9780791887011. DOI: 10.1115/GT2023-103873. [Online]. Available: https://asmedigitalcollection.asme.org/GT/proceedings/GT2023/87011/V07BT14A023/1168137.

[34] Phadke, U. and Owen, J., "Aerodynamic aspects of the sealing of gas-turbine rotor-stator systems: Part 1: The behavior of simple shrouded rotating-disk systems in a quiescent environment," *International Journal of Heat and Fluid Flow*, vol. 9, no. 2,

pp. 98–105, Jun. 1, 1988, ISSN: 0142-727X. DOI: 10.1016/0142-727X(88)90060-4. [Online]. Available: https://www.sciencedirect.com/science/article/pii/0142727X88900604.

[35] Phadke, U. and Owen, J., "Aerodynamic aspects of the sealing of gas-turbine rotor-stator systems: Part 2: The performance of simple seals in a quasi-axisymmetric external flow," *International Journal of Heat and Fluid Flow*, vol. 9, no. 2, pp. 106–112, Jun. 1, 1988, ISSN: 0142-727X. DOI: 10.1016/0142-727X(88)90061-6. [Online]. Available: https://www.sciencedirect.com/science/article/pii/0142727X88900616.

[36] Phadke, U. and Owen, J., "Aerodynamic aspects of the sealing of gas-turbine rotor-stator systems: Part 3: The effect of nonaxisymmetric external flow on seal performance," *International Journal of Heat and Fluid Flow*, vol. 9, no. 2, pp. 113–117, Jun. 1, 1988, ISSN: 0142-727X. DOI: 10.1016/0142-727X(88)90062-8. [Online]. Available: https://www.sciencedirect.com/science/article/pii/0142727X88900628.

[37] Owen, J. M., "An approximate solution for the flow between a rotating and a stationary disk," *Journal of Turbomachinery*, vol. 111, no. 3, pp. 323–332, Jul. 1, 1989, ISSN: 0889-504X. DOI: 10.1115/1.3262275. [Online]. Available: https://doi.org/10.1115/1.3262275.